Am J Transl Res 2023;15(9):5850-5872
www.ajtr.org /ISSN:1943-8141/AJTR0146317

Original Article

Integrative analysis of cellular autophagy-related genes in steroid-induced osteonecrosis of the femoral head

Yu Wang[1*], Yuke Zhang[1*], Hongxu Lu[1], Kai Liu[1], Wanxiong He[1], Zhiwei Pei[1], Jianzhong Wang[2]

[1]Inner Mongolia Medical University, Hohhot 010050, Inner Mongolia, China; [2]Department of Orthopedics and Traumatology, The Second Affiliated Hospital of Inner Mongolia Medical University, Hohhot 010030, Inner Mongolia, China. [*]Co-first authors.

Received September 4, 2022; Accepted September 11, 2023; Epub September 15, 2023; Published September 30, 2023

Abstract: Objective: This study aimed to identify and evaluate genes associated with cellular autophagy in steroid hormonal femoral head necrosis. Methods: Autophagy-related differentially expressed genes (ARDEGs) in steroid-induced osteonecrosis of the femoral head (SONFH) were identified by obtaining the intersection of differentially expressed genes (DEGs) and autophagy-related genes in a SONFH Gene Expression Omnibus dataset. The ARDEGs were screened, and correlations between gene expression and immune cell infiltration were evaluated. Finally, the validation of hub genes was undertaken through quantitative real-time-PCR. Results: A comparison of peripheral blood samples from patients with and without SONFH revealed 189 DEGs. Gene Ontology, Kyoto Encyclopedia of Genes and Genomes, and gene set enrichment analyses showed that the DEGs were related to various biologic processes (e.g., neutrophil activation) and pathways (e.g., hematopoietic cell lineage). The expression levels of these genes were correlated with the infiltration of multiple immune cell types. Among the 189 putative autophagy-related genes associated with SONFH, three genes, *RPL6*, *RPL9*, and *RPL23*, were identified as candidate biomarkers or therapeutic targets based on network analysis and their correlations with immune cell subtypes. The quantitative real-time polymerase chain reaction results confirmed our prediction regarding the mRNA expression of RPL9 and RPS6. Conclusion: In this study, we identified 189 putative autophagy-related genes associated with SONFH, and the prediction of down-regulated genes RPL9 and RPS6 was validated using PCR, thereby expanding our understanding of the contribution of autophagy to SONFH.

Keywords: Steroid-induced osteonecrosis, femoral head, autophagy, integrative analysis, qRT-PCR

Introduction

Overuse of glucocorticoids can cause the active component of the femoral head to degenerate, resulting in steroid-induced osteonecrosis of the femoral head (SONFH). The resulting femoral head deterioration and collapse cause hip pain and dysfunction [1, 2]. Although the precise pathophysiology of SONFH is unknown, several pathogenetic hypotheses have been proposed, including disorders of lipid metabolism, abnormal differentiation of bone marrow mesenchymal stem cells, apoptosis, inadequate blood supply, and genetic polymorphisms [3-6].

Autophagy is a widespread catabolic process in which eukaryotic cells engulf and encapsulate cytoplasmic proteins or organelles in vesicles. Subsequently, these vesicles fuse with lysosomes to generate autophagic lysosomes that break down the lysosomal contents. Autophagy is similar to apoptosis and is associated with hormonal femoral necrosis and other pathologic processes. For example, a rapamycin analog that induced autophagy slowed tumor formation in PTEN-deficient mice by inhibiting the activity of mTOR [7]. Pancreatic stellate cells can feed on tumor tissues by secreting alanine released by autophagy [8]. A study on the effect of altered autophagic activity on osteogenic differentiation of the bone marrow MSCs revealed that the autophagy activator rapamycin increased autophagic activity and inhibited osteogenic differentiation [9]. Studies using a rat model and cultured osteoblasts indicated that the PI3K/Akt/mTOR autophagy signaling pathway might suppress the development of

osteoporosis by boosting osteoblast proliferation, differentiation, and bone production [10].

Autophagy-related genes associated with SONFH have not yet been identified, thereby necessitating further research. Bioinformatics-based screening studies for predicting cellular autophagy in SONFH are insufficient. In this study, we used a bioinformatics-based approach to identify the genes associated with cellular autophagy in hormonal femoral head necrosis, thus laying the framework for further mechanistic studies. The GSE123568 dataset was obtained based on a genome-wide microarray analysis of peripheral blood samples collected from 30 patients with SONFH and 10 controls to establish genetic biomarkers for SONFH diagnosis. After analyzing the GSE123568 data and generating a protein-protein interaction (PPI) network, correlations between hub genes and various immune cell infiltrates as well as between immune cells and immunologic subtypes were evaluated. The study results improve our understanding of the role of autophagy in SONFH, which will serve as a guide for future studies and provide a basis for the diagnosis and treatment of SONFH.

Materials and methods

Data sources and pre-processing

The GEOquery package of R (version 4.1.1, http://r-project.org/) [11] was used to download data from the Gene Expression Omnibus (GEO) database (https://www.ncbi.nlm.nih.gov/geo/). The GSE123568 dataset of femoral head necrosis expression profiles (*Homo sapiens*, data platform GPL15207) was retrieved. The dataset included 40 samples, of which 30 were obtained from the peripheral blood serum of patients with SONFH, and 10 samples were obtained from controls without SONFH. All 40 samples were included in this study. The raw data from the GSE123568 dataset were read using the GEOquery package, and a gene expression matrix was generated after background signal removal and data normalization. Intersample comparisons were performed using boxplots.

Analysis of immune cell infiltration

Single-sample gene set enrichment analysis (ssGSEA), a variant of gene set enrichment analysis (GSEA), enables estimation of an enrichment score that reflects the absolute enrichment of gene sets in each sample within a dataset [12]. We used the Gene Ontology (GSVA) package [13] to evaluate the infiltration of 28 immune cell types and displayed the infiltration in each sample, and heat maps created using the pheatmap package (https://CRAN.R-project.org/package=pheatmap).

CIBERSORT [14] uses the concept of linear support vector regression to deconstruct transcriptome expression matrix [15]. We used the CIBERSORT algorithm to evaluate the gene expression matrix data to determine the infiltration of 22 immune cell types. Samples with *p*-values less than 0.05 were removed to obtain the immune cell infiltration matrix. The corrplot package [16] was used to generate a heat map of the correlations.

Construction of immune subtype and identification of differentially expressed genes (DEGs)

The immune signatures in femoral head necrosis were assessed using the ConsensusClusterPlus [17] and Rtsne [18] packages, and subtypes were visualized using ggplot2 package [19]. DEGs between several immune subtypes were screened using the limma package [20]. To visualize the DEGs, volcano maps were generated using the ggplot2 package, and heat maps were generated using the pheatmap package. DEGs with $P < 0.05$ and $|logFC| > 0.5$ were included in the analysis.

Functional enrichment analysis

Gene Ontology (GO) analysis is used extensively in large-scale functional enrichment studies to evaluate the function of DEGs in three general categories: biologic process (BP), molecular function (MF), and cellular component (CC). The Kyoto Encyclopedia of Genes and Genomes (KEGG) database is a comprehensive source of data on genomes, biological pathways, diseases, and drugs. The intersection between DEGs and autophagy-related genes in the Human Gene Database (GeneCards) (https://www.genecards.org/) was obtained, and the identified genes were subjected to independent GO annotation and KEGG pathway analyses using the clusterProfiler package [21]. A *p* value less than 0.05 was regarded as significant.

The intersecting genes were then subjected to GSEA with "c2.cp.kegg.v7.0.entrez.gmt" as the reference gene set and $P < 0.05$ as the threshold for significance. The gene expression matrix was subjected to GSVA, and $P < 0.05$ was considered significant enrichment.

Construction of PPI network and hub gene screening

The intersection of DEGs and autophagy-related genes was entered into the STRING database (https://string-db.org/) [22] for PPI network construction. The results were visualized using Cytoscape 3.8.2 [23]. Hub genes were screened using the MCODE plug-in. The ggpubr package (https://CRAN.R-project.org/package=ggpubr) was used to visualize the relationships between hub gene expression and immune cell infiltration and immune subtypes.

Cell line culture

The specialized complete cell medium and PBS buffer were pre-warmed using a water bath set at 37°C; note that trypsin does not require a water bath. We employed microscopy to assess cell condition and capture images; the criterion for passaging is the attainment of an 80% cell fusion rate. Old medium was removed, 2 ml of PBS buffer was introduced, and we endeavored to eliminate deceased cells and residual medium with thoroughness by performing this procedure twice.

We applied 1 ml of trypsin to sufficiently cover the culture vessel's base and incubated the vessel in the cell incubator for 35 seconds to facilitate digestion. Upon removal from the incubator, cells were observed under the microscope. When they assumed a rounded form and exhibit indications of detachment, we promptly introduced 3 ml of complete medium to cease digestion. We employed a pipette gun to gently dislodge cells from the vessel's base, aspirating 100 μl into a sterile EP tube. Subsequently, we introduced 900 μl of culture medium, combining it through gentle pipetting. We transfered 20 μl to an automated cell counting plate. 30 readings were performed using the cell counter and the average was calculated from three measurements to minimize inaccuracies.

With the aid of a pipette gun, we aspirated the cells from the vessel's base and transfered them into a 15 ml centrifuge tube. They were centrifuged at 1000 rpm for 5 minutes. Supernatant was removed, followed by adding 1 ml of culture medium for gentle resuspension. Cells were passaged into a fresh petri dish at a 1:3 ratio. 10 ml of medium were added to the petri dish, and the dish was agitated vertically ten times to promote uniform cell distribution. The dish was labeled with the cell's name, culture initiation date, and generation number. For subsequent experiments, we focused on generations 2 to 4.

Cell viability assay

MC3T3-E1 cells were seeded at a density of 2500 cells per well in a 96-well plate, with 6 replicate wells. To mitigate edge effects, 200 μl of PBS buffer was added to each well along the outer edges. Cells at passages 2-4 in a healthy growth state were selected, and they were treated with different groups: complete growth medium or complete growth medium containing varying concentrations of DEX.

Group assignments were as follows: A: Blank control group with 0 cells per well, supplemented with 100 μl of complete growth medium. B: Experimental control group with 2500 cells per well, supplemented with 100 μl of complete growth medium. C: Experimental group with 2500 cells per well, treated with DEX concentrations of 1, 10, 100, 200, and 300 μM/L in 100 μl of complete growth medium each.

Following a 24-hour incubation with DEX, the old culture medium was discarded from the 96-well plate, and pipette tips were changed between groups. Each well received 90 μL of complete growth medium and 10 μl of CCK-8 reagent, followed by a 3-hour light-protected incubation in a culture chamber. Post-incubation, the OD values for each well were measured at a wavelength of 450 nm using a microplate reader. Cell viability was calculated based on the OD values, where cell survival percentage = $[(C - A)/(B - A)] \times 100\%$. Ultimately, the half maximal inhibitory concentration (IC_{50}) was determined as the optimal DEX concentration for inducing the MC3T3-E1 cell line's response.

Extraction of total RNA, reverse transcription, and quantitative real-time PCR

500 μl of Trizol was added to the cellular samples and incubated for 5 minutes to achieve complete cell lysis. The lysate was transferred

Table 1. Reverse transcription system configuration

Component	Utilization rate
Total RNA	3.0 μg
OligodT primer	2.5 μL
RNase-free water	Up to 12.5 μL
70°C, 5 min	
RT Buffer	4.0 μL
dNTPS	2.0 μL
RT Enzyme	1.0 μL
RI Enzyme	0.5 μL
Total volume	20.0 μL
42°C, 60 min; 70°C, 10 min	

Table 2. Reaction cycle settings

Temperature	Time
25°C	10 min
42°C	60 min
85°C	5 s

to 1.5 ml EP tubes. To each tube, we introduced 100 μl of chloroform, and vigorously shook the tubes for 15 seconds to ensure thorough mixing. The mixture stood at room temperature for 5 minutes, followed by centrifugation in a low-temperature centrifuge set at 4°C, 12000 rpm for 10 minutes. This centrifugation resulted in the formation of three distinct liquid layers: the upper layer, containing colorless RNA; the middle layer, consisting of a white protein layer; and the lower layer, the red organic phase. Subsequently, we extracted the upper aqueous phase and transfered it to a sterile EP tube. An equivalent volume of isopropanol was added to the tube, mixed through oscillation, and left at room temperature for 10 minutes. The mixture was then centrifuged at 4°C, 12000 rpm for 10 minutes. Following centrifugation, we discarded the supernatant, and introduced 1 ml of 75% ethanol to wash and resuspend the precipitate. The suspension was once again centrifuged at 4°C, 700 rpm for 5 minutes, with the supernatant being discarded. The precipitate was then air-dried at room temperature for 10 minutes and preserved. For complete RNA dissolution, we introduced 25 μl of DEPC water to the EP tube. The total RNA concentration wa subsequently determined using a UV spectrophotometer.

To generate cDNA, reverse transcription was conducted employing the cDNA RevertAid Reverse Transcriptase (#EP0441). The formulation of the reaction system is detailed in **Table 1**, while the reaction settings are delineated in **Table 2**. The resulting cDNA was subsequently diluted and reserved for further analysis.

Table 3. Amplification system configuration

Component	Volume
SYBR Green I mix (2 ×)	5.0 μL
Primer-F (10 μM)	0.2 μL
Primer-R (10 μM)	0.2 μL
cDNA	0.2 μL
Sterilized distilled water	Up to 10.0 μL

The gene quantification analysis was conducted using the PerfectStart Green qPCR SuperMix (#AQ601-04) assay kit on an ABI7500 fluorescence quantitative PCR instrument. GAPDH was employed as the internal reference, and the reaction system was prepared at a volume of 10 ml. The mRNA expression levels were determined using the $2^{-\Delta\Delta Ct}$ method. Details of the amplification system can be found in **Table 3**, amplification program settings are provided in **Table 4**, and the thermal cycling conditions are outlined in **Table 5**. Primer sequences are provided in **Table 6**.

Statistical analysis

R (version 4.1.1, http://r-project.org/) was used for all data processing and statistical analyses. Independent Student's *t*-tests were used to compare continuous variables, and the Mann-Whitney U-test was used to assess the differences between non-normally distributed variables (i.e., Wilcoxon rank sum test). The threshold for significance was $P < 0.05$, and all tests were two-sided.

Results

Study flow

A flow chart of the study is shown in **Figure 1A**. The gene expression matrix for the GSE123568 dataset was background-corrected, and the data were normalized. Data, before and after correction, are summarized in boxplots (**Figure 1B**, **1C**).

Analysis of immune cell infiltration

We used the ssGSEA algorithm to evaluate the correlations between serum markers of femo-

Table 4. Amplification program setup schedule

Cycle	Steps	Temperature	Time	Explanation
1	1	94°C	30 s	Initial template denaturation
40	1	94°C	5 s	Template Degeneration
	2	60°C	15 s	Annealing
	3	72°C	10 s	Extension

Table 5. Melting program setting schedule

Cycle	Temperature	Time
1	95°C	15 s
	60°C	60 s
	95°C	1 s

Table 6. Primer sequences

Target Name	Primer (5'→3')
m-Gapdh-128-F	AGCCCAAGATGCCCTTCAGT
m-Gapdh-128-R	CCGTGTTCCTACCCCCAATG
m-Rpl6-F	AGAAGGCTACGCTCCAGCATCA
m-Rpl6-R	CAGTCACAAGCAGCAAGCCACT
m-Rpl9-F	CATCAACGTGGAGCTGAGTCTTC
m-Rpl9-R	GACCGCATCTTGTATCGGAAGC
m-Rpl23-F	ACGGCTGAACAGACTTCCTGCT
m-Rpl23-R	ACTGTGCAAGGCGTTCTTCTCG
m-Eef1b2-F	GTAGAAGACACCACAGGAAGTGG
m-Eef1b2-R	ACTGTGCAAGGCGTTCTTCTCG
m-Rpl7-F	TGAGAGGCATCTCTATCAAGTTGC
m-Rpl7-R	GCTTCAGCATCTCCTTGGTGTC
m-Rpl26-F	AGGCTAATGGCACAACCGTCCA
m-Rpl26-R	CTTGGCTTTCCTCTCCAGGATC
m-Rps6-F	TGTCCGCCAGTATGTTGTCAGG
m-Rps6-R	CACGAGGAGTAACAAGTCGCTG
m-Rps3a1-F	GGTACGATGTGAAAGCTCCAGC
m-Rps3a1-R	GGCTCACTTCAAACACACGACC
m-Rpl7-F	TCGCAGAGTTGAAGGTGAAGCG
m-Rpl7-R	CCATCCGAATCTCAGTGCGGTA
m-Psma3-F	GTTTGCTGGCAGATGCTCGTTC
m-Psma3-R	CAGCCAAAAGGTCTAACAGCGC
m-Npm1-F	GCACATTAGTGGACAGCATCTAG
m-Npm1-R	GTTACCACCTCCAGGAGCAGAT
m-RPL39-F	CTTCTCCATTCCTCCGCCATC
m-RPL39-R	TCGTTCTCCTCCAGTGTCTTCT

ral head necrosis and infiltrates of multiple immune cell types (**Figure 2A**). The relative frequencies of several immune cell types differed between the femoral head necrosis and control groups, such as MDSCs and plasmacytoid dendritic cells. The frequency of central memory CD4+ T cells was significantly higher ($P < 0.05$) in the femoral head necrosis group than in the control group (**Figure 2B-O**).

DEGs between two immune type clusters and visualization of immune subtypes

Patients with femoral head necrosis were divided into two subtypes according to their immunologic characteristics (**Figure 3A**), and the DEGs between the two subtypes were evaluated. Visualization using volcano plots and heat maps revealed 462 DEGs, including 350 and 112 genes with upregulated and downregulated expressions, respectively, in the group with femoral head necrosis (**Figure 3B**, **3C**). Additionally, 189 autophagy-related differentially expressed genes (ARDEGs) were identified among the 462 DEGs (**Figure 3D**).

Functional enrichment analysis of autophagy-related DEGs

Results of the GO and KEGG analyses of the ARDEGs are summarized in **Figures 4**, **5**, S1, S2, S3 and **Tables 7**, **8**. GO analysis revealed that the ARDEGs were enriched in neutrophil activation, ficolin-1-rich granule, and cytokine receptor activity. KEGG pathway analysis revealed that ARDEGs are involved in hematopoietic cell lineage, HIF-1 signaling pathway, and inflammatory bowel disease pathways.

GSEA and GSVA

The intersection of all genes and ARGs yielded 6,371 genes, which were evaluated by GSEA and GSVA (**Figure 6**; **Table 9**). GSEA revealed enrichment in pathways related to the ribosome and Fc gamma R-mediated phagocytosis, and the GSVA results showed that the pathways were primarily clustered in GSE3982 neutrophils vs. Th1 cells (upregulated), reactome signaling by NOTCH2, and acylglycerol *O*-acyltransferase activity, as well as 10 additional pathways.

PPI network and hub gene analyses

The 189 ARDEGs were subjected to a PPI network analysis (**Figure 7A**), and two subgroups were identified using the MCODE plug-in, Cluster 1 (*RPL6*, *RPL9*, *RPL23*, *EEF1B2*, *NPM1*, *RPS17*, *RPL26*, *RPS6*, *RPL39*, *RPS3A*, *RPL7*, and *PSMA3*) and Cluster 2 (*TLR2*, *CXCR1*, *TREM1*, *TLR8*, *IL1R1*, *IL6R*, *TLR4*, *CXCR2*, *CXCL10*, *MMP9*, *IL1R2*, and *ITGAX*), for a total of 24 hub genes (**Figure 7B**, **7C**). The top 12

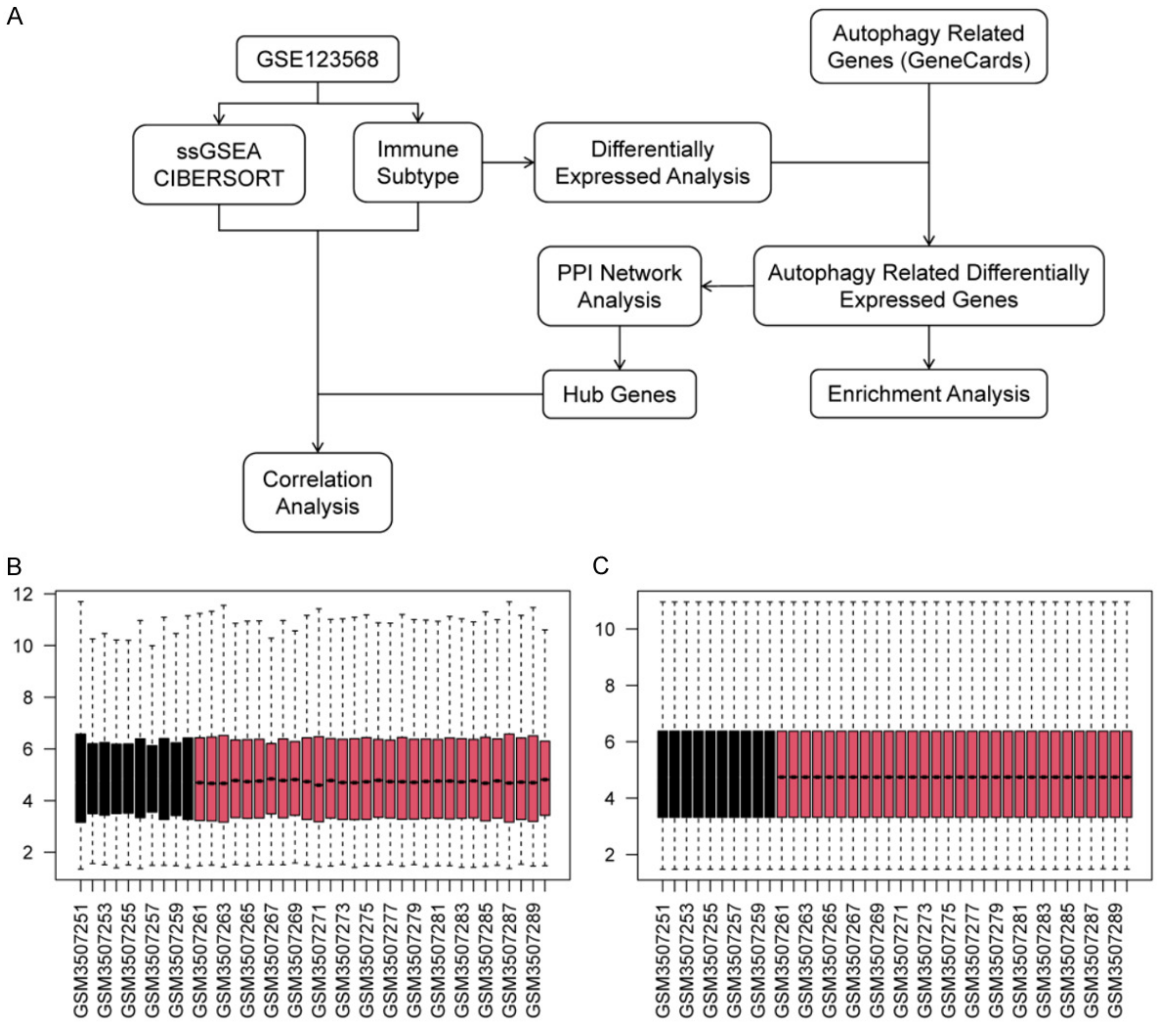

Figure 1. Study flow chart (A) and boxplots of the GSE123568 dataset before (B) and after (C) correction.

genes were obtained by the MCC algorithm using the cytoHubba [24] plug-in: *RPL6*, *RPL9*, *RPL23*, *EEF1B2*, *NPM1*, *RPS17*, *RPL26*, *RPS6*, *RPL39*, *RPS3A*, *RPL7*, and *PSMA3*. The network consisted of 12 nodes and 62 edges, consistent with the 12 genes in Cluster 1 obtained using the MCODE plug-in.

Immune cell infiltration and correlations between immune cell infiltration and immune subtypes

We used the CIBERSORT algorithm to assess alterations in immune cell infiltrates in patients with femoral head necrosis. Neutrophil and macrophage subpopulations accounted for a large proportion of infiltrating immune cells (**Figure 8A**). We detected correlations between infiltrates of multiple immune cell types, which are shown in **Figure 8B**, where purple represents a positive correlation and sky blue represents a negative correlation. The two immune subtypes differed in the relative frequencies of monocytes, neutrophils, activated NK cells, T cells CD4 memory activated, and T cells CD8 (**Figure 8C-F**).

Correlations between hub gene expression, immune cell infiltration, and immune subtypes

An analysis of the 24 hub genes in the immune subtypes revealed 13 genes, whose expression levels were relatively high in Cluster 1 than in Cluster 2 (*RPL6*, *RPL9*, *RPL23*, *EEF182*, *NPM1*, *RPS17*, *RPL26*, *RPS6*, *RPL39*, *RPS3A*, *RPL7*, *PSMA3*, and *CXCL10*) and 11 genes, whose expression levels were relatively high in Cluster 2 than in Cluster 1 (*TLR2*, *CXCR1*, *TREM1*,

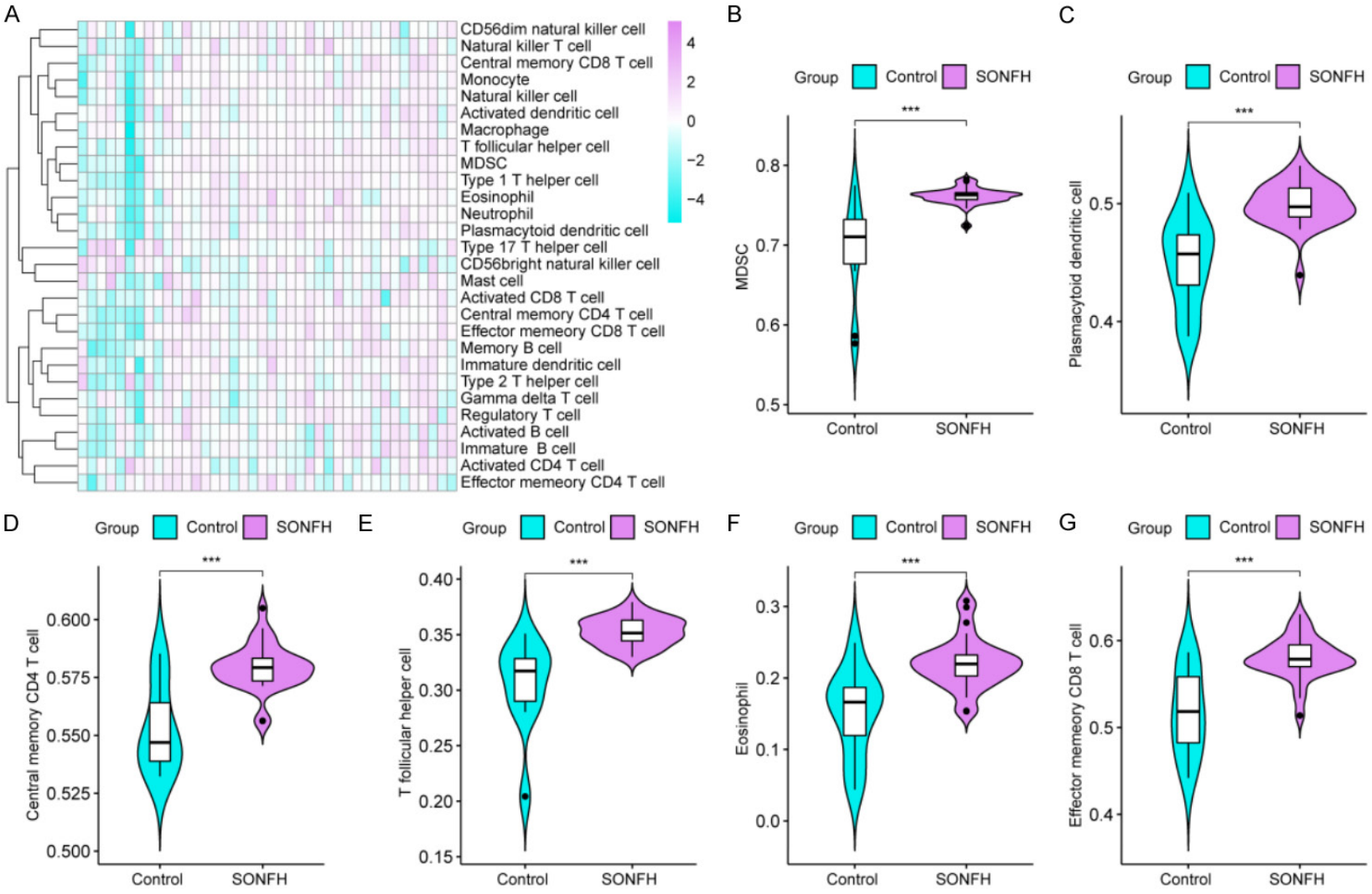
A
CD56dim natural killer cell
Natural killer T cell
Central memory CD8 T cell
Monocyte
Natural killer cell
Activated dendritic cell
Macrophage
T follicular helper cell
MDSC
Type 1 T helper cell
Eosinophil
Neutrophil
Plasmacytoid dendritic cell
Type 17 T helper cell
CD56bright natural killer cell
Mast cell
Activated CD8 T cell
Central memory CD4 T cell
Effector memeory CD8 T cell
Memory B cell
Immature dendritic cell
Type 2 T helper cell
Gamma delta T cell
Regulatory T cell
Activated B cell
Immature B cell
Activated CD4 T cell
Effector memeory CD4 T cell
4
2
0
−2
−4
B
Group Control SONFH
***
MDSC
0.8
0.7
0.6
0.5
Control SONFH
C
Group Control SONFH
***
Plasmacytoid dendritic cell
0.5
0.4
Control SONFH
D
Group Control SONFH
***
Central memory CD4 T cell
0.600
0.575
0.550
0.525
0.500
Control SONFH
E
Group Control SONFH
***
T follicular helper cell
0.40
0.35
0.30
0.25
0.20
0.15
Control SONFH
F
Group Control SONFH
***
Eosinophil
0.3
0.2
0.1
0.0
Control SONFH
G
Group Control SONFH
***
Effector memeory CD8 T cell
0.6
0.5
0.4
Control SONFH

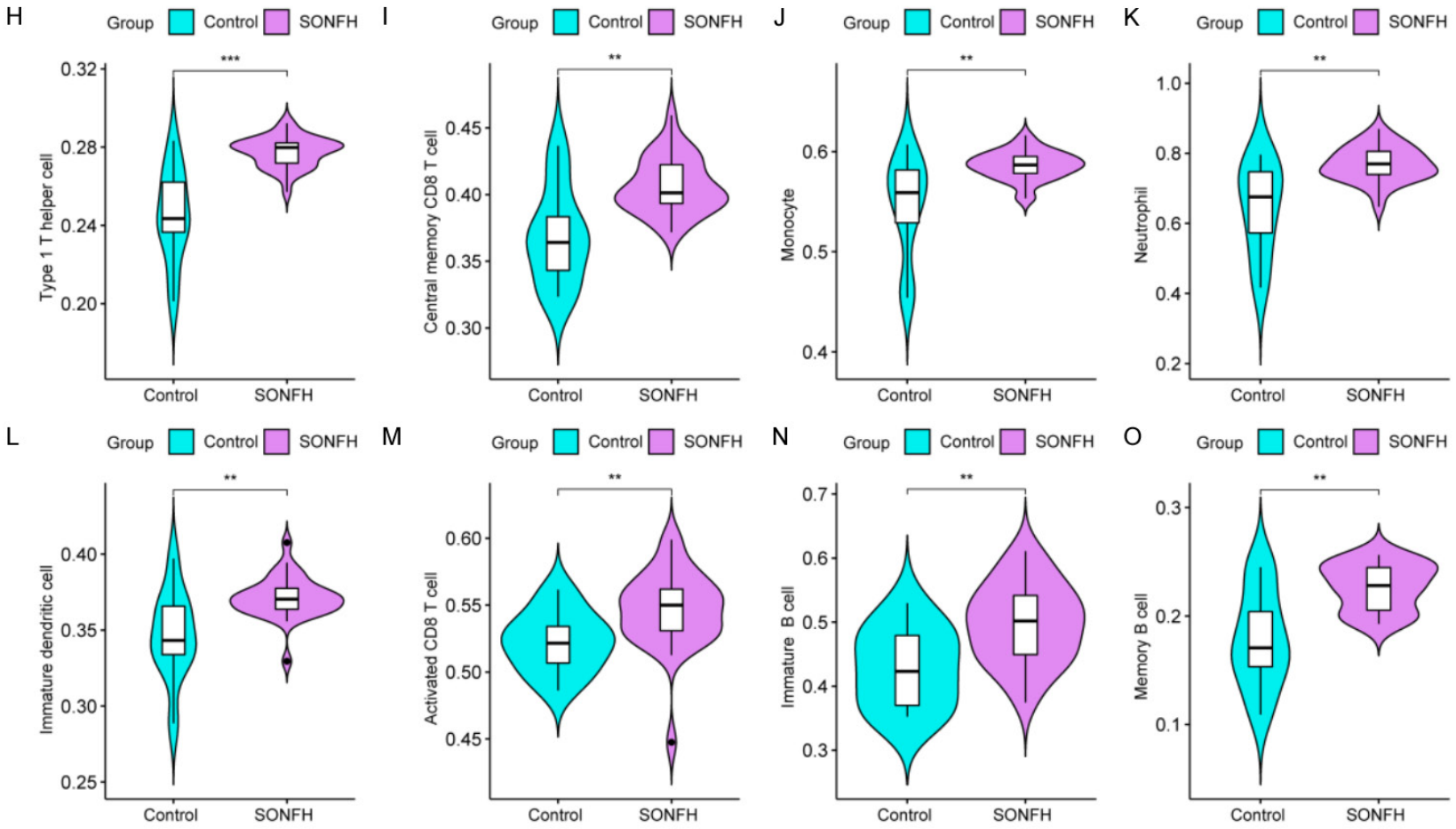

Figure 2. Single-sample gene set enrichment analysis (ssGSEA) and immune cell analysis. A. Heat map of infiltrates of 28 immune cell types; fuchsia indicates a positive correlation, and sky blue indicates a negative correlation. B-O. Differences in immune cell frequencies between the femoral head necrosis and control groups. Fuchsia and sky blue indicate the femoral head necrosis and control groups, respectively (ns: $P > 0.05$, *$P < 0.05$, **$P < 0.01$, ****$P < 0.0001$).

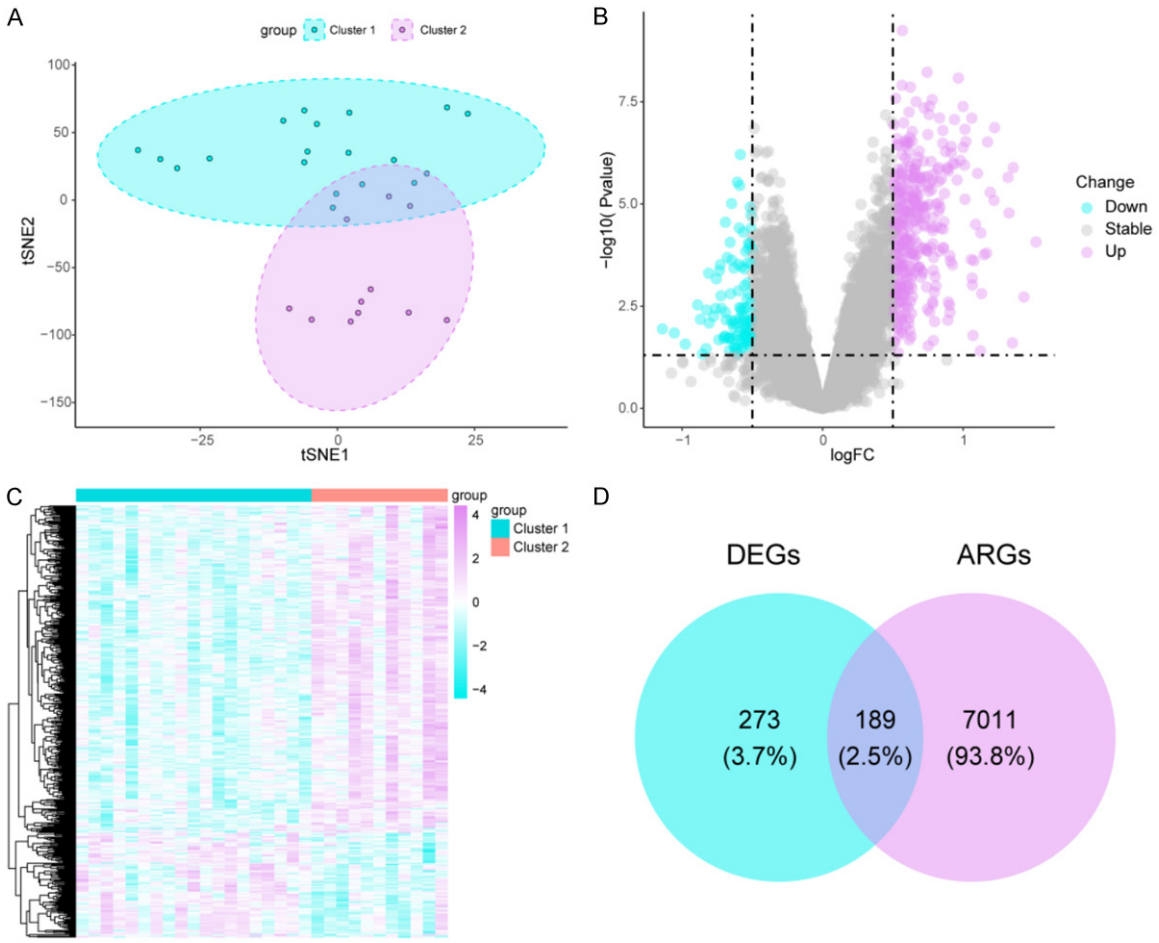

Figure 3. Identification of immune subtypes and visualization of differentially expressed genes (DEGs). A. Identification of immune subtypes: subtype 1 (Cluster 1) is shown in sky blue, and subtype 2 (Cluster 2) is shown in violet. B. Volcano plot showing DEGs in the two subtypes. Genes whose expressions are upregulated in the femoral head necrosis group are shown in violet, and genes whose expressions are downregulated are shown in blue. C. Heat map showing DEGs between the two subtypes. D. Venn diagram showing the intersection between DEGs and autophagy-related genes (ARGs).

TLR8, *IL1R1*, *IL6R*, *TLR4*, *CXCR2*, *MMP9*, *IL1R2*, and *ITGAX*) (**Figure 9A**).

The expression levels of several hub genes were correlated with immune cell infiltrates ($R \geq 0.6$, $P < 0.05$). *CXCR1*, *CXCR2*, *IL1R1*, *IL1R2*, *IL6R*, *ITGAX*, *MMP9*, *TLR4*, *TLR8*, and *TREM1* were associated with neutrophils; *CXCL10* was associated with monocytes; and *NPM1* was significantly associated with naïve B cells (**Figure 9B-M**).

Validation of differentially expressed autophagy-related hub genes

In vitro cellular and molecular biology experiments were performed to verify the accuracy of the constructed model. Using the mouse pre-osteoblast MC3T3-E1 cell line, DEX was added to mimic hormonal stimulation-induced osteonecrosis of the femoral head. To determine what dose of DEX was added as the appropriate induction concentration, CCK-8 experiments with different DEX drug gradients were performed to examine the cell viability status. It was found that cell viability decreased by more than 50% after 24 hours of DEX (300 μM) treatment. Therefore, 200 μM DEX was chosen as the condition for subsequent experiments to assess the mRNA expression levels of key 12 genes in the NC and DEX groups using qRT-PCR (**Figure 10A-L**). The relative expression of *RPL9* and *RPS6* in mouse osteoblast MC3T3-E1 cells of the drug group was significantly reduced

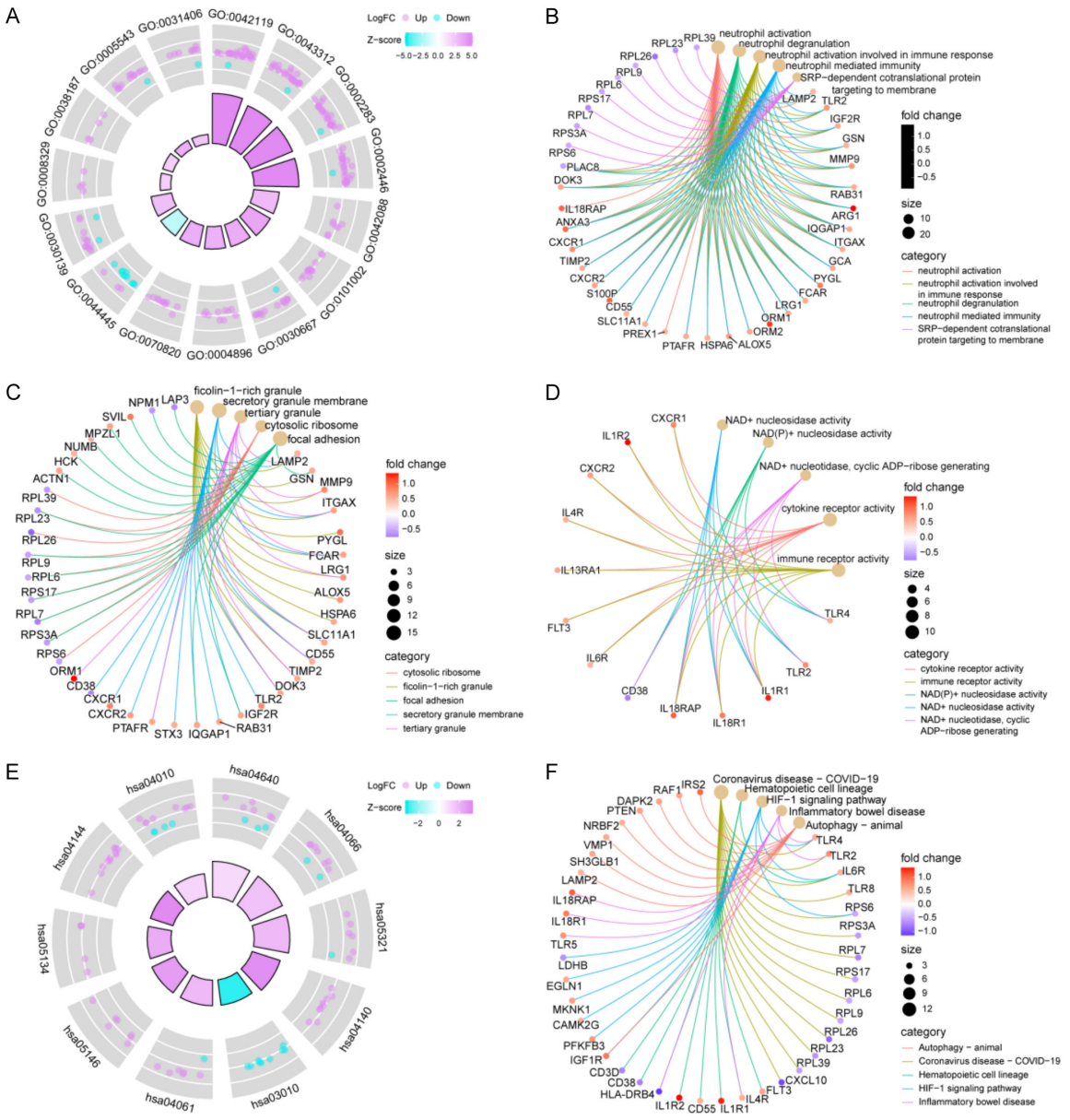

Figure 4. Functional analysis of the autophagy-related differentially expressed genes (ARDEGs). A. Circular plot of the Gene Ontology (GO) enrichment results. Violet dots represent genes with upregulated expressions, and sky blue dots represent genes with downregulated expressions; the more intense the color, the smaller the Z-score. B-D. Retinotopic plots of the biologic process (BP), molecular function (MF), and cellular component (CC) results from the GO analysis. E. Circular plots of the Kyoto Encyclopedia of Genes and Genomes (KEGG) pathway enrichment results. Darker purple indicates a larger Z-score, darker blue indicates a smaller Z-score, purple-red dots indicate genes with upregulated expressions, and sky blue dots indicate genes with downregulated expressions. F. Retinotopic plot of the KEGG analysis results.

compared to the control group. The relative expression of *RPS17* and *RPL7* was significantly higher in MC3T3-E1 cells of mouse osteoblasts in the drug group compared to the control group.

Discussion

In steroid-induced osteonecrosis of the femoral head (SONFH), the active component of the femoral head degenerates as a result of long-

A

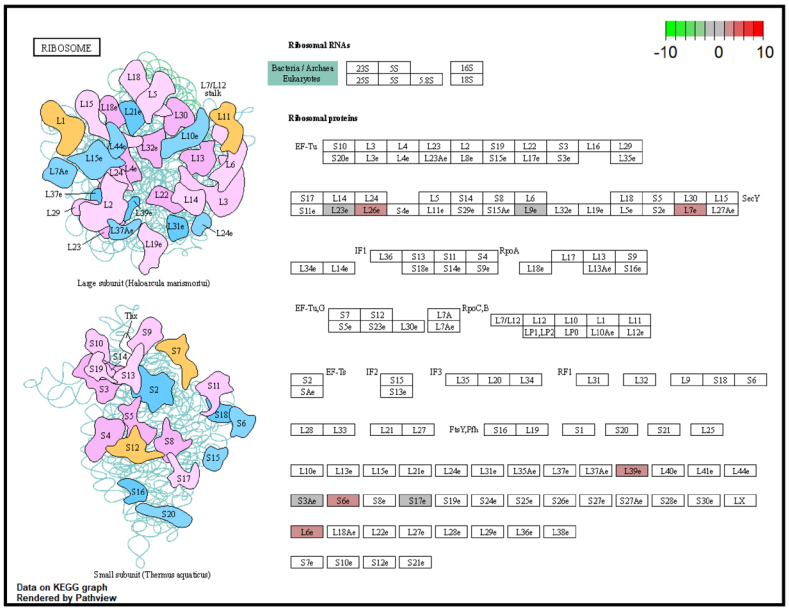

B

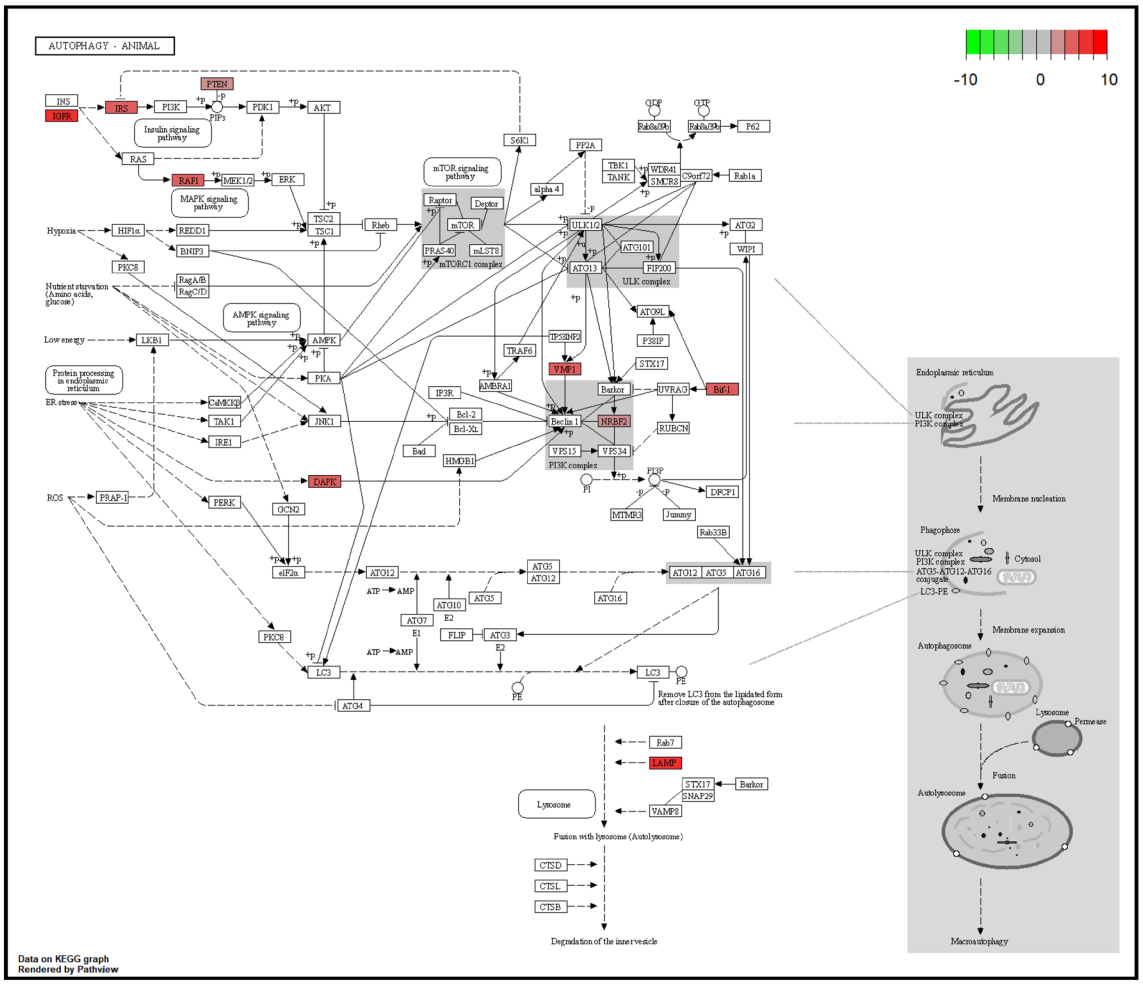

Figure 5. Pathway diagrams. A. Ribosome pathway. B. Autophagy-animal pathway. Colors indicate differential expression; red denotes genes with upregulated expression, and green denotes genes with downregulated expression.

Table 7. GO enrichment analysis results

ONTOLOGY	ID	Description	*p*-value	p.adjust	q-value	Count
BP	GO:0042119	Neutrophil activation	8.61E-15	3.16E-11	2.39E-11	29
BP	GO:0043312	Neutrophil degranulation	2.11E-13	3.00E-10	2.26E-10	27
BP	GO:0002283	Neutrophil activation involved in immune response	2.45E-13	3.00E-10	2.26E-10	27
BP	GO:0002446	Neutrophil mediated immunity	4.15E-13	3.81E-10	2.88E-10	27
BP	GO:0006614	SRP-dependent cotranslational protein targeting to membrane	8.44E-07	0.000619996	0.000468626	9
BP	GO:0071900	Regulation of protein serine/threonine kinase activity	1.51E-06	0.00069424	0.000524743	18
BP	GO:0042088	T-helper 1 type immune response	2.61E-06	0.00086954	0.000657244	6
BP	GO:0042110	T cell activation	3.91E-06	0.001104362	0.000834736	17
BP	GO:0001819	Positive regulation of cytokine production	5.88E-06	0.001438557	0.001087338	16
BP	GO:0006605	Protein targeting	6.59E-06	0.001440502	0.001088808	16
CC	GO:0101002	Ficolin-1-rich granule	2.45E-08	8.27E-06	5.64E-06	13
CC	GO:0030667	Secretory granule membrane	2.29E-07	3.87E-05	2.64E-05	15
CC	GO:0070820	Tertiary granule	4.80E-07	5.41E-05	3.69E-05	11
CC	GO:0022626	Cytosolic ribosome	8.19E-07	6.92E-05	4.72E-05	9
CC	GO:0005925	Focal adhesion	2.35E-06	0.000132014	9.00E-05	16
CC	GO:0030055	Cell-substrate junction	2.91E-06	0.000132014	9.00E-05	16
CC	GO:0060205	Cytoplasmic vesicle lumen	2.91E-06	0.000132014	9.00E-05	14
CC	GO:0031983	Vesicle lumen	3.12E-06	0.000132014	9.00E-05	14
CC	GO:0030139	Endocytic vesicle	7.73E-06	0.000290345	0.000198024	13
CC	GO:0034774	Secretory granule lumen	1.29E-05	0.000434764	0.000296523	13
MF	GO:0003953	NAD+ nucleosidase activity	6.71E-09	1.31E-06	9.39E-07	6
MF	GO:0050135	NAD(P)+ nucleosidase activity	6.71E-09	1.31E-06	9.39E-07	6
MF	GO:0061809	NAD+ nucleotidase, cyclic ADP-ribose generating	6.71E-09	1.31E-06	9.39E-07	6
MF	GO:0004896	Cytokine receptor activity	4.55E-08	6.64E-06	4.78E-06	10
MF	GO:0140375	Immune receptor activity	1.10E-06	0.000128433	9.24E-05	10
MF	GO:0005543	Phospholipid binding	1.23E-05	0.000900916	0.000647919	16
MF	GO:1901981	Phosphatidylinositol phosphate binding	5.61E-05	0.003275435	0.002355621	9
MF	GO:0038187	Pattern recognition receptor activity	7.33E-05	0.003856658	0.002773624	4
MF	GO:0003735	Structural constituent of ribosome	8.33E-05	0.003856658	0.002773624	9
MF	GO:0031406	Carboxylic acid binding	9.86E-05	0.003856658	0.002773624	9

Table 8. KEGG pathway analysis results

ID	Description	*p*-value	p.adjust	q-value	Count
hsa05171	Coronavirus disease - COVID-19	1.59E-05	0.002891434	0.002590845	14
hsa04640	Hematopoietic cell lineage	2.39E-05	0.002891434	0.002590845	9
hsa04066	HIF-1 signaling pathway	5.15E-05	0.004066407	0.00364367	9
hsa05321	Inflammatory bowel disease	6.72E-05	0.004066407	0.00364367	7
hsa04140	Autophagy - animal	0.000370304	0.017922733	0.016059517	9
hsa03010	Ribosome	0.000847944	0.033311562	0.029848551	9
hsa04061	Viral protein interaction with cytokine and cytokine receptor	0.00097967	0.033311562	0.029848551	7
hsa05146	Amoebiasis	0.001101209	0.033311562	0.029848551	7
hsa05134	Legionellosis	0.001963381	0.049694748	0.044528569	5
hsa04144	Endocytosis	0.002053502	0.049694748	0.044528569	11
hsa04010	MAPK signaling pathway	0.002272464	0.049994204	0.044796894	12

term or short-term heavy glucocorticoid use, resulting in hip pain and dysfunction caused by deterioration of the femoral head and collapse [25]. SONFH seriously affects patients' quality of life and carries a familial and social burden. Current treatment for collapsed-stage femoral head necrosis is total hip arthroplasty. However, artificial joint prosthetics have limited service life, and prosthetic revision is difficult. The precise pathophysiology of SONFH is yet unknown; however, it may involve disorders of lipid metabolism, abnormal differentiation of bone marrow mesenchymal stem cells, programmed cell death, insufficient blood supply, and genetic

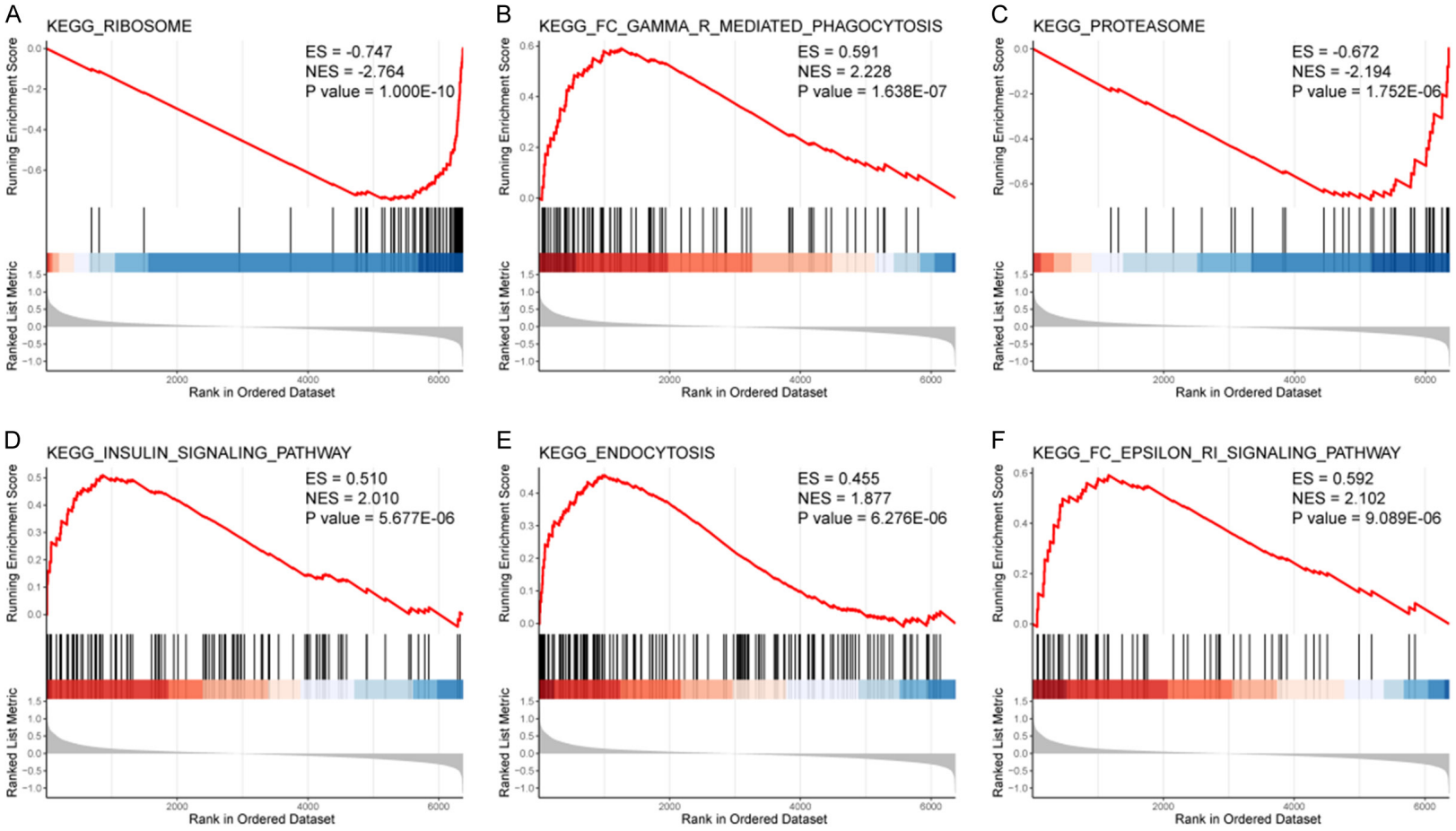
A
KEGG_RIBOSOME
ES = -0.747
NES = -2.764
P value = 1.000E-10
B
KEGG_FC_GAMMA_R_MEDIATED_PHAGOCYTOSIS
ES = 0.591
NES = 2.228
P value = 1.638E-07
C
KEGG_PROTEASOME
ES = -0.672
NES = -2.194
P value = 1.752E-06
D
KEGG_INSULIN_SIGNALING_PATHWAY
ES = 0.510
NES = 2.010
P value = 5.677E-06
E
KEGG_ENDOCYTOSIS
ES = 0.455
NES = 1.877
P value = 6.276E-06
F
KEGG_FC_EPSILON_RI_SIGNALING_PATHWAY
ES = 0.592
NES = 2.102
P value = 9.089E-06
Running Enrichment Score
Ranked List Metric
Rank in Ordered Dataset

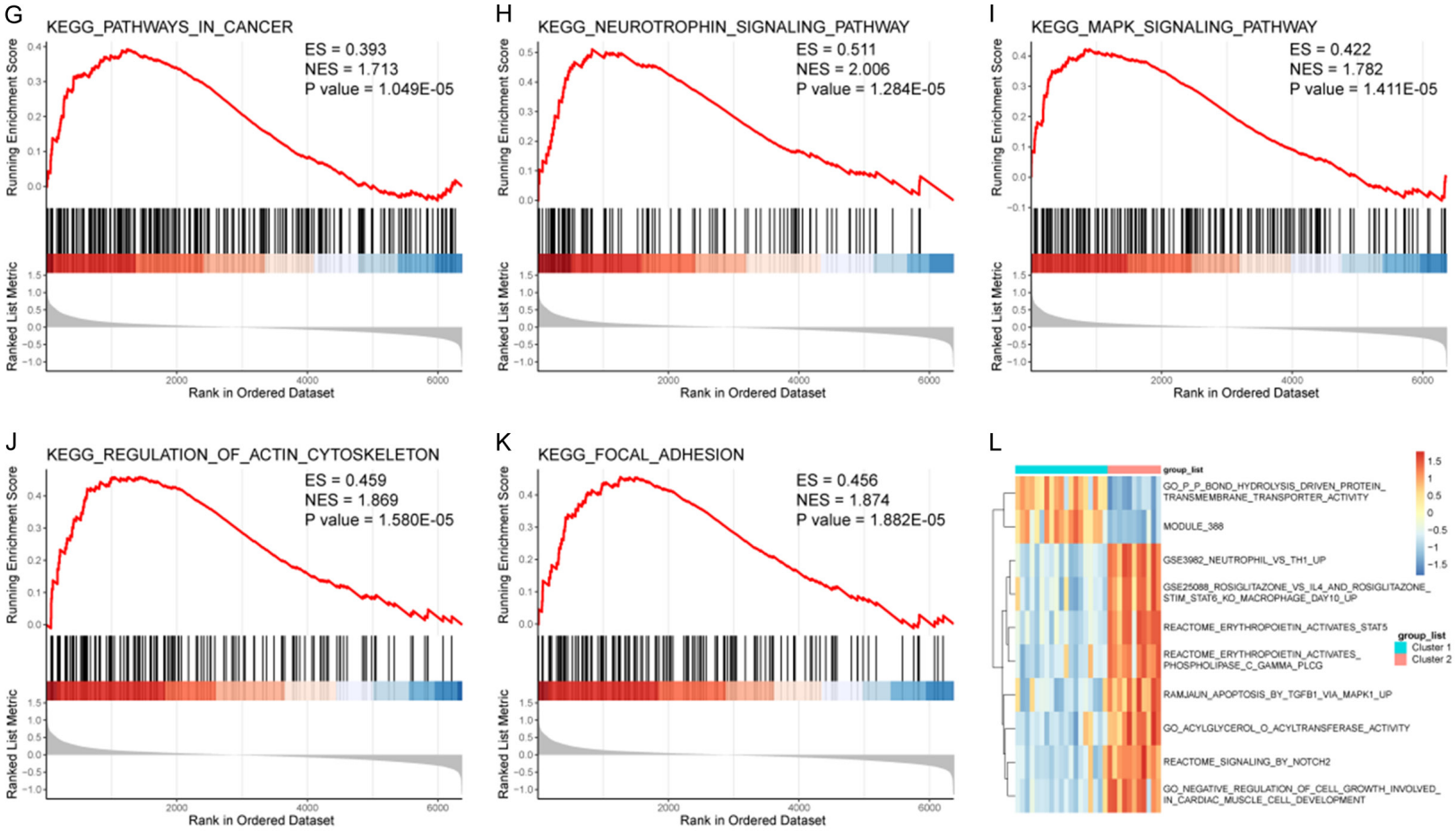

Figure 6. Gene set enrichment analysis (GSEA) and GSVA results. A total of 11 pathways were identified in the (A-K) GSEA, and 10 pathways were identified in the (L) GSVA.

Table 9. GSEA results

ID	EnrichmentScore	NES	*p*-value	p.adjust	q-value
KEGG_RIBOSOME	-0.746679177	-2.76442461	1.00E-10	1.49E-08	8.32E-09
KEGG_FC_GAMMA_R_MEDIATED_PHAGOCYTOSIS	0.590787842	2.2283412	1.64E-07	1.22E-05	6.81E-06
KEGG_PROTEASOME	-0.672196919	-2.193777621	1.75E-06	8.70E-05	4.86E-05
KEGG_INSULIN_SIGNALING_PATHWAY	0.509566474	2.010302008	5.68E-06	0.000187027	0.000104381
KEGG_ENDOCYTOSIS	0.45542503	1.877395201	6.28E-06	0.000187027	0.000104381
KEGG_FC_EPSILON_RI_SIGNALING_PATHWAY	0.591981818	2.102097539	9.09E-06	0.000223216	0.000124578
KEGG_PATHWAYS_IN_CANCER	0.392742361	1.712763743	1.05E-05	0.000223216	0.000124578
KEGG_NEUROTROPHIN_SIGNALING_PATHWAY	0.510726291	2.00611238	1.28E-05	0.000233674	0.000130415
KEGG_MAPK_SIGNALING_PATHWAY	0.421850694	1.781502776	1.41E-05	0.000233674	0.000130415
KEGG_REGULATION_OF_ACTIN_CYTOSKELETON	0.458889367	1.869174108	1.58E-05	0.000233945	0.000130566
KEGG_FOCAL_ADHESION	0.455683904	1.874117046	1.88E-05	0.000233945	0.000130566
KEGG_LEUKOCYTE_TRANSENDOTHELIAL_MIGRATION	0.540440866	2.042514302	2.02E-05	0.000233945	0.000130566
KEGG_ERBB_SIGNALING_PATHWAY	0.546087231	2.035700469	2.04E-05	0.000233945	0.000130566
KEGG_PYRUVATE_METABOLISM	-0.690513231	-2.064179165	9.02E-05	0.000838979	0.00046824
KEGG_ACUTE_MYELOID_LEUKEMIA	0.601300009	2.076168867	9.10E-05	0.000838979	0.00046824
KEGG_EPITHELIAL_CELL_SIGNALING_IN_HELICOBACTER_PYLORI_INFECTION	0.542520204	1.966734025	9.42E-05	0.000838979	0.00046824
KEGG_B_CELL_RECEPTOR_SIGNALING_PATHWAY	0.573056954	2.02552732	9.57E-05	0.000838979	0.00046824

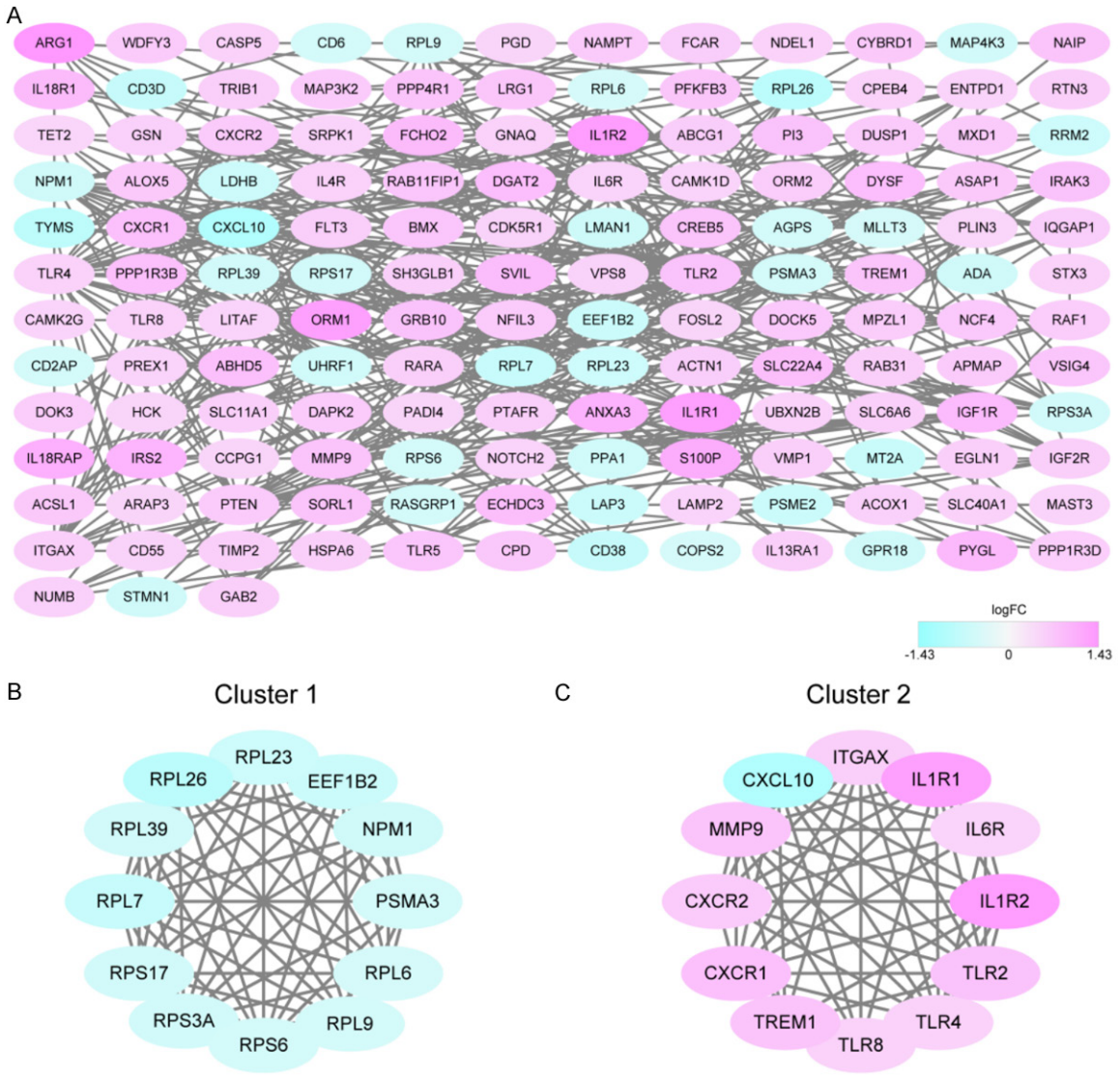

Figure 7. Protein-protein interaction network and hub gene screening. A. Protein interaction analysis of 189 autophagy-related differentially expressed genes (ARDEGs). B, C. Gene screening using Cytoscape identified two subclusters, and each subcluster contained 12 hub genes, for a total of 24 hub genes. Pink indicates genes with upregulated expression, and sky blue indicates genes with downregulated expression; darker colors indicate a larger |logFC| value than those of lighter colors.

polymorphism [3-5]. The adverse effects of glucocorticoids on osteoblasts, osteoclasts, and osteocytes can be alleviated by autophagy, a type of programmed cell death, and genes that control homeostatic processes linked to tissue dynamics actively influence programmed cell death [6].

Few studies have explored autophagy-related genes in hormonal femoral head necrosis, and little is known regarding the roles of individual autophagy-related genes in pathogenesis and treatment, including the effects on bone homeostasis and osteoporosis. A comprehensive bioinformatic analysis of the autophagy-related genes involved in the pathogenesis of SONFH revealed some candidate genes [26]; however, the study was limited by the amount of genetic data in the human autophagy database. Using a broader dataset, the DEGs in the GSE123568 dataset that were ARGs in GeneCards, we identified 189 potential ARDEGs associated with SONFH, including 34 and 155 genes with downregulated and upregulated

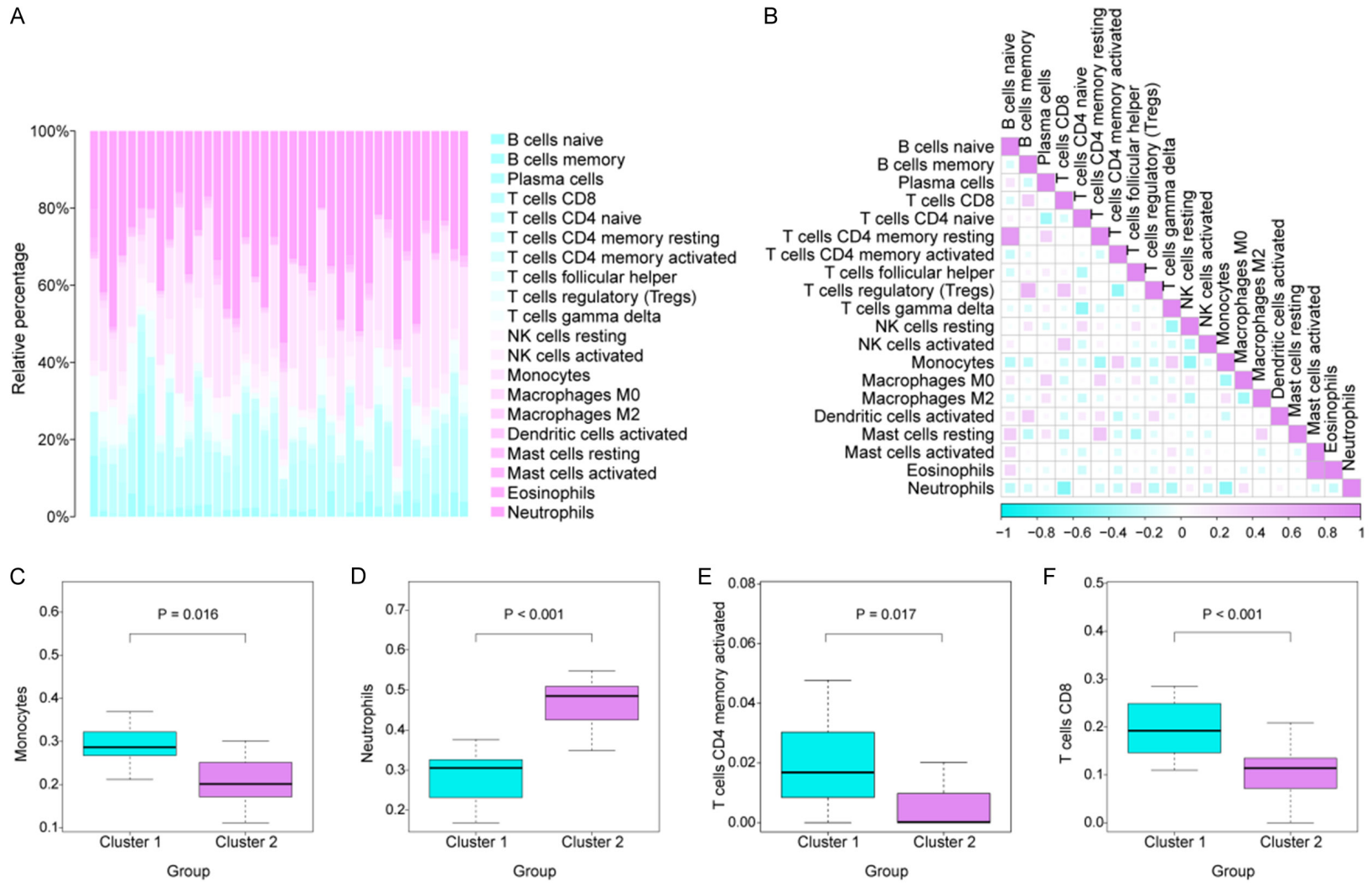

Figure 8. Immune cell infiltration analysis and correlations between immune cell infiltrates and immune signature subtypes. A. Bar plot of immune cell infiltration in patients. B. Heat map of the correlations between the infiltration of 22 immune cell types. Fuchsia denotes a positive correlation, and sky blue indicates a negative correlation. C-F. Box plots of the differences in four immune cell types between the two immune subtypes; sky blue is Cluster 1, and fuchsia is Cluster 2.

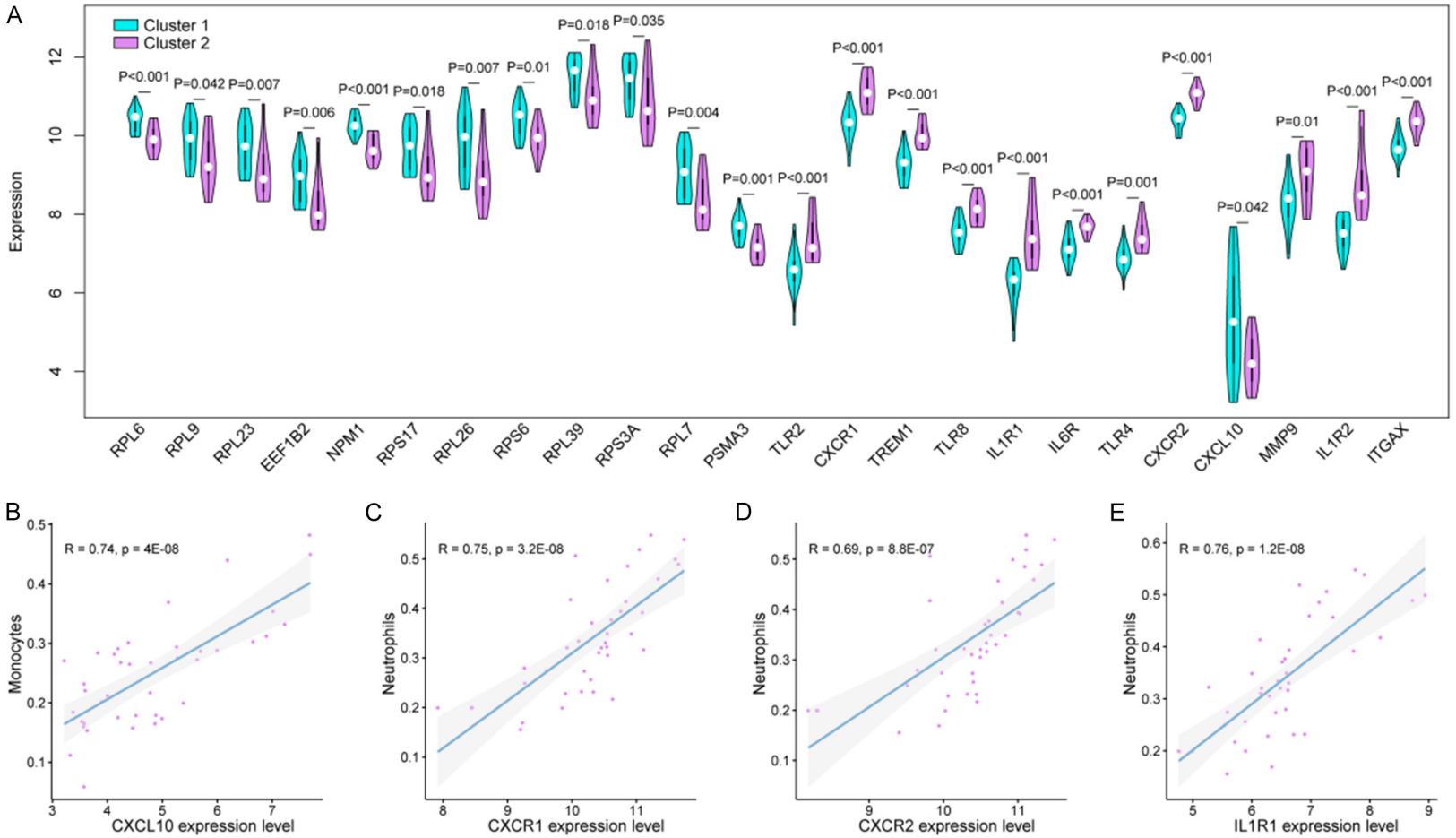
A
Cluster 1
Cluster 2
Expression
P<0.001
P=0.042
P=0.007
P=0.006
P<0.001
P=0.018
P=0.007
P=0.01
P=0.018
P=0.035
P=0.004
P=0.001
P<0.001
P<0.001
P<0.001
P<0.001
P<0.001
P<0.001
P<0.001
P=0.001
P<0.001
P=0.042
P=0.01
P<0.001
P<0.001
RPL6
RPL9
RPL23
EEF1B2
NPM1
RPS17
RPL26
RPS6
RPL39
RPS3A
RPL7
PSMA3
TLR2
CXCR1
TREM1
TLR8
IL1R1
IL6R
TLR4
CXCR2
CXCL10
MMP9
IL1R2
ITGAX
B
R = 0.74, p = 4E-08
Monocytes
CXCL10 expression level
C
R = 0.75, p = 3.2E-08
Neutrophils
CXCR1 expression level
D
R = 0.69, p = 8.8E-07
Neutrophils
CXCR2 expression level
E
R = 0.76, p = 1.2E-08
Neutrophils
IL1R1 expression level

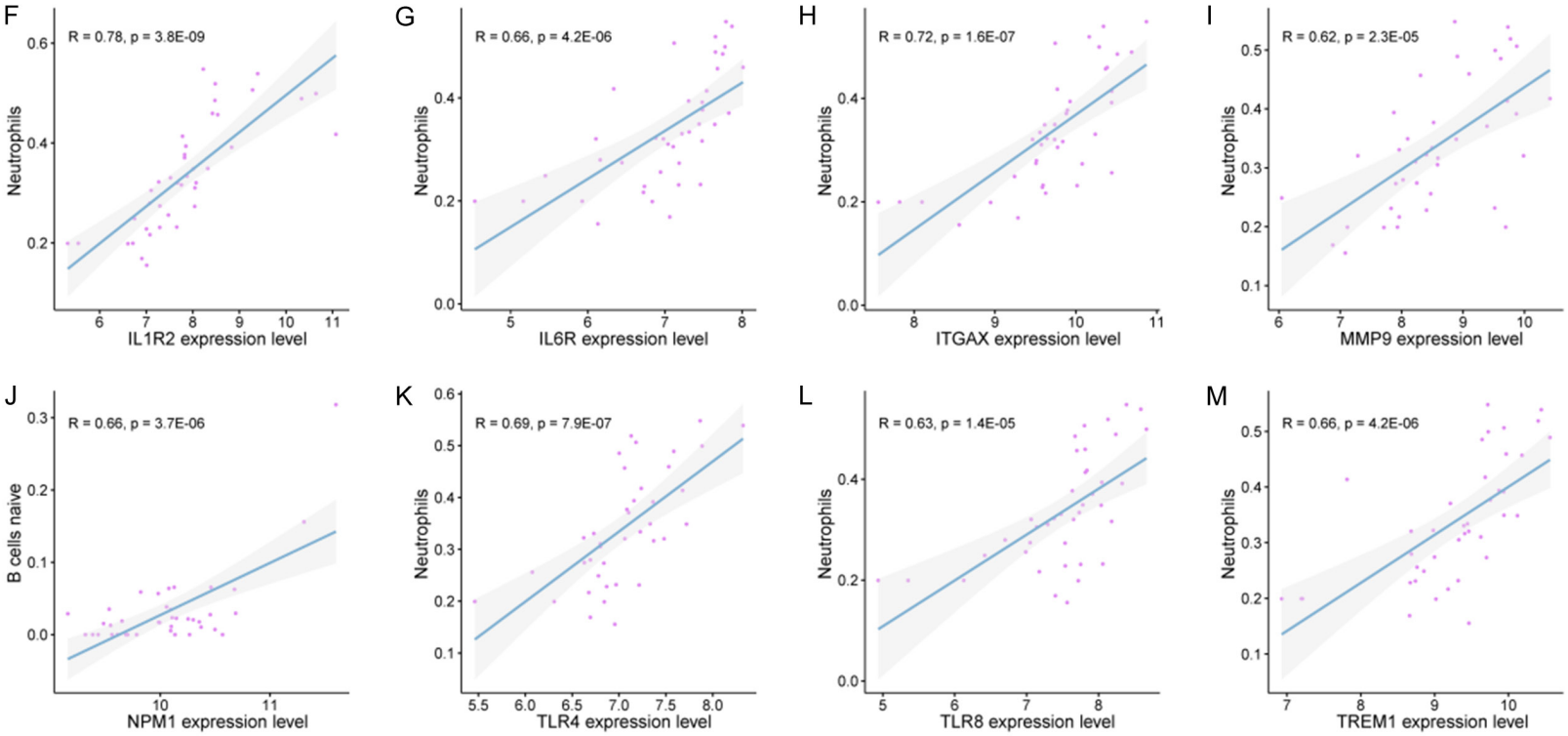

Figure 9. Correlation analysis between hub genes, immune subtypes, and immune cells. A. Violin plot of the differential expression of 24 hub genes between immune subtypes; Cluster 1 is shown in sky blue, and Cluster 2 is shown in purple. B-M. Scatter plots of the correlations between 12 hub genes and different immune cell types. Differences were considered significant at $P < 0.05$.

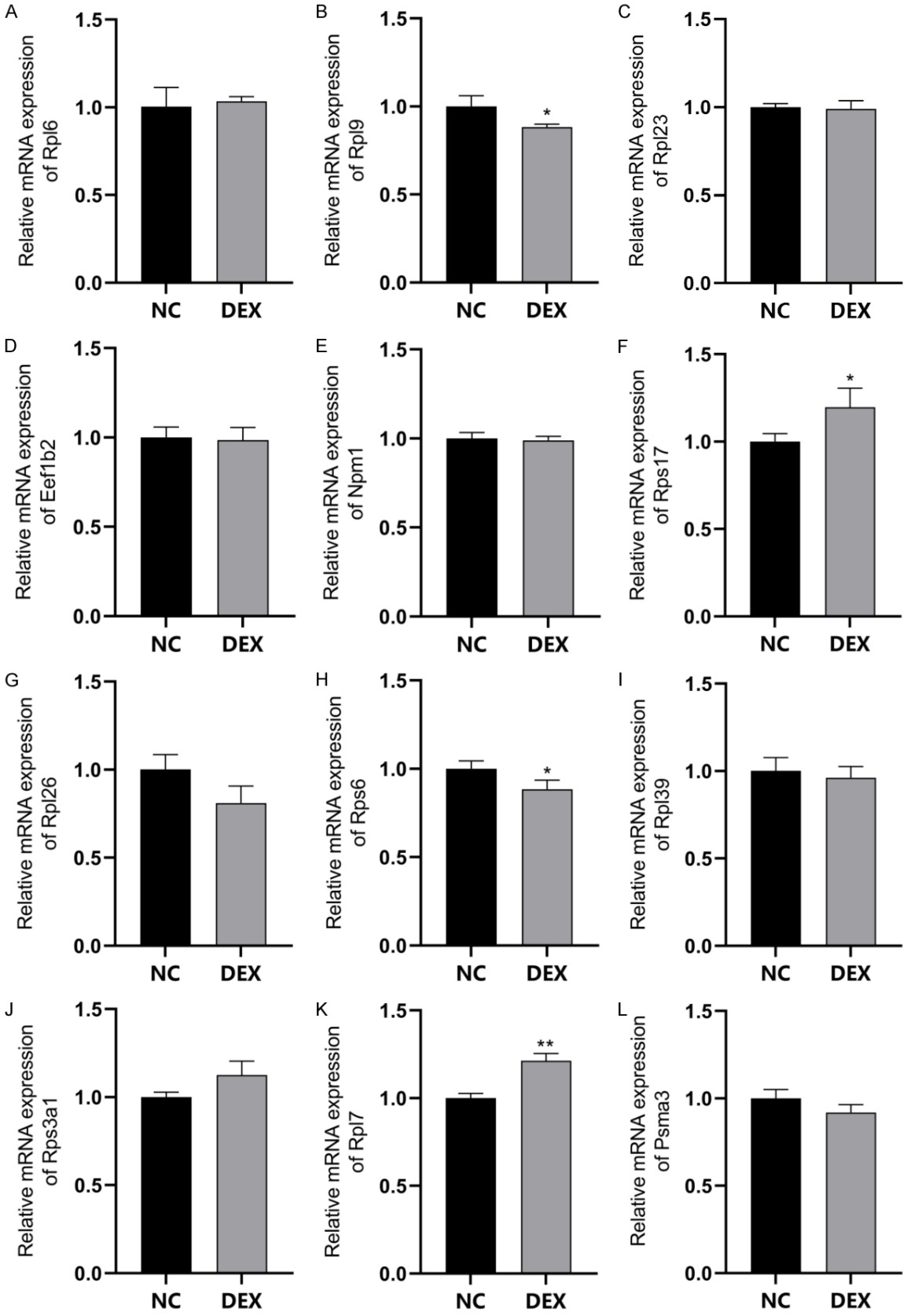

Figure 10. Validation evaluation of the 12 hub genes. A-L. Results qRT-PCR showed that the relative expressions of *RPL9* and *RPS6* were also significantly decreased in drug groups compared to controls. The relative expressions of *RPS17* and *RPL7* were significantly increased in drug groups compared to controls.

expressions, respectively. Some ARDEGs involved in the differential expression of autophagy-associated genes in ONFH have been investigated previously. For example, the expression levels of MMP9, a matrix metalloproteinase that degrades and destroys extracellular matrix components and is closely associated with tumor infiltration and metastasis, were reduced in patients with nontraumatic osteonecrosis of the femoral head, and eight SNPs, including SNPs in MMP-9, showed promise as diagnostic serum markers [27]. Li et al. [28] constructed a diagnostic model for SONFH based on eight genes, including *PTEN*, *PAK1*, and *TLR4*, and showed that these genes are involved in pathologic processes, such as autophagy and bone metabolism, in a study involving 60 patients with SONFH. Additional studies are required to identify candidate ARDEGs in SONFH and construct a comprehensive molecular network for SONFH.

We evaluated the biologic functions of the 34 autophagy-related genes that were differentially expressed in SONFH. According to the GO analysis, the ARDEGs were tightly linked to the biological processes of neutrophil activation, ficolin-1-rich granules, and cytokine receptor function. A correlation between neutrophil activation and bone destruction was found in a study by Ceglie et al. [29], i.e., neutrophils produce substances that stimulate osteoclast resorption activity, leading to bone destruction. KEGG enrichment analysis showed that the ARDEGs were enriched in hematopoietic cell lineage, HIF-1 signaling pathway, and inflammatory bowel disease pathways. Although autophagy induction by the above pathways has not been associated with osteoclast homeostasis, Wan et al. [30] examined the regulation of angiogenesis via HIF-1α, which subsequently regulates osteoclastogenesis. Thus, the identified ARDEGs may be involved in the pathogenesis of SONFH. However, more studies are needed to validate our results and provide a complete picture of the biologic functions of these ARDEGs in SONFH.

We evaluated the newly identified ARDEGs using a PPI network analysis and revealed the biological mechanisms associated with the network using the MCODE cytoHubba plug-in. Twelve hub genes associated with autophagy were identified (*RPL6*, *RPL9*, *RPL23*, *EEF1B2*, *NPM1*, *RPS17*, *RPL26*, *RPS6*, *RPL39*, *RPS3A*, *RPL7*, and *PSMA3*), and two subgroups were identified. Cluster 1 consisted of 12 nodes and 62 edges. Furthermore, we confirmed our prediction that the drug group showed significantly reduced expression of the RPL9 and RPS6 genes compared to the control group using PCR analysis with mouse osteoblasts MC3T3-E1 cells. Numerous studies have focused on the connections among these continuously expressed genes and inflammatory, autoimmune, and neurodegenerative disorders. For example, Wang et al. [31] showed that PSMA1 and PSMA3 play key roles in protein homeostasis, and Watanabe et al. [32] demonstrated that RPL9 encodes a novel damage-associated molecular pattern molecule with a regulatory role in the inflammatory response. However, only a few comprehensive genetic studies have focused on the relationship between SONFH and autophagy. The genes we identified provide a basis for understanding the relationship between autophagy and SONFH.

Although our bioinformatic-based study successfully identified potential autophagy-related genes associated with SONFH, it has some limitations. First, GSE123568 is the only dataset in the GEO database on patients with SONFH; hence, the sample size was relatively small. Second, cellular, animal, and human studies are required to confirm the differentially expressed marker genes associated with autophagy and the underlying mechanisms. Although further studies are needed to address these limitations, the results of this study advance our knowledge of the genes contributing to cellular autophagy in hormonal femoral head necrosis. In addition to offering direction for the clinical diagnosis and treatment of SONFH, our study identified candidate biomarkers and regulatory mechanisms linking autophagy to SONFH.

Conclusion

A bioinformatic analysis identified 189 potential autophagy-related genes associated with SONFH, including *RPL6*, *RPL9*, *RPL23*, *EEF1B2*, *NPM1*, *RPS17*, *RPL26*, *RPS6*, *RPL39*, *RPS3A*, *RPL7*, and *PSMA3*, which may be drug targets or biomarkers. Our predictions for the downregulated genes *RPL9* and *RPS6* were validated using PCR. These findings increase our

understanding of the molecular mechanisms underlying SONFH and provide guidance for further studies aimed at validating the role of autophagy in SONFH and developing diagnostic tools and therapy.

Acknowledgements

This study was funded by National Natural Science Foundation of China (NSFC; No. 81860401) to Jianzhong Wang, and Inner Mongolia Autonomous Region Science and Technology Program Project (No. 2022YFSH0075) to Jianzhong Wang.

Disclosure of conflict of interest

None.

Address correspondence to: Dr. Jianzhong Wang, Department of Orthopedics and Traumatology, The Second Affiliated Hospital of Inner Mongolia Medical University, Hohhot 010030, Inner Mongolia, China. Tel: +86-0417-2576293; E-mail: wangjianzhongwj@163.com

References

[1] Herndon JH and Aufranc OE. Avascular necrosis of the femoral head in the adult. A review of its incidence in a variety of conditions. Clin Orthop Relat Res 1972; 86: 43-62.

[2] Mwale F, Wang H, Johnson AJ, Mont MA and Antoniou J. Abnormal vascular endothelial growth factor expression in mesenchymal stem cells from both osteonecrotic and osteoarthritic hips. Bull NYU Hosp Jt Dis 2011; 69 Suppl 1: S56-61.

[3] Luo H, Lan W, Li Y, Lian X, Zhang N, Lin X and Chen P. Microarray analysis of long-noncoding RNAs and mRNA expression profiles in human steroid-induced avascular necrosis of the femoral head. J Cell Biochem 2019; 120: 15800-15813.

[4] Wang A, Ren M and Wang J. The pathogenesis of steroid-induced osteonecrosis of the femoral head: a systematic review of the literature. Gene 2018; 671: 103-109.

[5] Zhang Y, Sun R, Zhang L, Feng L and Liu Y. Effect of blood biochemical factors on nontraumatic necrosis of the femoral head: logistic regression analysis. Orthopade 2017; 46: 737-743.

[6] Qi Y, Wang J, Sun M, Ma C, Jin T, Liu Y, Cao Y and Wang J. MMP-14 single-nucleotide polymorphisms are related to steroid-induced osteonecrosis of the femoral head in the population of northern China. Mol Genet Genomic Med 2019; 7: e00519.

[7] Podsypanina K, Lee RT, Politis C, Hennessy I, Crane A, Puc J, Neshat M, Wang H, Yang L, Gibbons J, Frost P, Dreisbach V, Blenis J, Gaciong Z, Fisher P, Sawyers C, Hedrick-Ellenson L and Parsons R. An inhibitor of mTOR reduces neoplasia and normalizes p70/S6 kinase activity in Pten+/- mice. Proc Natl Acad Sci U S A 2001; 98: 10320-10325.

[8] Sousa CM, Biancur DE, Wang X, Halbrook CJ, Sherman MH, Zhang L, Kremer D, Hwang RF, Witkiewicz AK, Ying H, Asara JM, Evans RM, Cantley LC, Lyssiotis CA and Kimmelman AC. Pancreatic stellate cells support tumour metabolism through autophagic alanine secretion. Nature 2016; 536: 479-483.

[9] Li J, Wang Q, Lin X and Li BZ. Effects of autophagy activity on osteogenic differentiation potential of bone marrow mesenchymal stem cells. J Huazhong Univ Sci Technol Med Sci J 2012; 41: 5.

[10] Xi JC, Zang HY, Guo LX, Xue HB, Liu XD, Bai YB and Ma YZ. The PI3K/AKT cell signaling pathway is involved in regulation of osteoporosis. J Recept Signal Transduct Res 2015; 35: 640-5.

[11] Davis S and Meltzer PS. GEOquery: a bridge between the Gene Expression Omnibus (GEO) and BioConductor. Bioinformatics 2007; 23: 1846-1847.

[12] Barbie DA, Tamayo P, Boehm JS, Kim SY, Moody SE, Dunn IF, Schinzel AC, Sandy P, Meylan E, Scholl C, Frohling S, Chan EM, Sos ML, Michel K, Mermel C, Silver SJ, Weir BA, Reiling JH, Sheng Q, Gupta PB, Wadlow RC, Le H, Hoersch S, Wittner BS, Ramaswamy S, Livingston DM, Sabatini DM, Meyerson M, Thomas RK, Lander ES, Mesirov JP, Root DE, Gilliland DG, Jacks T and Hahn WC. Systematic RNA interference reveals that oncogenic KRAS-driven cancers require TBK1. Nature 2009; 462: 108-112.

[13] Hänzelmann S, Castelo R and Guinney J. GSVA: gene set variation analysis for microarray and RNA-seq data. BMC Bioinformatics 2013; 14: 7.

[14] Chen B, Khodadoust MS, Liu CL, Newman AM and Alizadeh AA. Profiling tumor infiltrating immune cells with CIBERSORT. Methods Mol Biol 2018; 1711: 243-259.

[15] Newman AM, Liu CL, Green MR, Gentles AJ, Feng W, Xu Y, Hoang CD, Diehn M and Alizadeh AA. Robust enumeration of cell subsets from tissue expression profiles. Nat Methods 2015; 12: 453-457.

[16] Wei T and Simko V. R package 'corrplot': visualization of a correlation matrix. 2021. Available from: https://github.com/taiyun/corrplot.

[17] Wilkerson MD and Hayes DN. ConsensusClusterPlus: a class discovery tool with confidence assessments and item tracking. Bioinformatics 2010; 26: 1572-1573.
[18] Krijthe JH. Rtsne: T-distributed stochastic neighbor embedding using a Barnes-Hut implementation. R package version 0.16. 2015. Available at https://github.com/jkrijthe/Rtsne.
[19] Wickham H. ggplot2: Elegant Graphics for Data Analysis. New York, NY: Springer-Verlag; 2016.
[20] Ritchie ME, Phipson B, Wu D, Hu Y, Law CW, Shi W and Smyth GK. limma powers differential expression analyses for RNA-sequencing and microarray studies. Nucleic Acids Res 2015; 43: e47.
[21] Wu T, Hu E, Xu S, Chen M, Guo P, Dai Z, Feng T, Zhou L, Tang W, Zhan L, Fu X, Liu S, Bo X and Yu G. clusterProfiler 4.0: a universal enrichment tool for interpreting omics data. Innovation (Camb) 2021; 2: 100141.
[22] von Mering C, Huynen M, Jaeggi D, Schmidt S, Bork P and Snel B. STRING: a database of predicted functional associations between proteins. Nucleic Acids Res 2003; 31: 258-261.
[23] Shannon P, Markiel A, Ozier O, Baliga NS, Wang JT, Ramage D, Amin N, Schwikowski B and Ideker T. Cytoscape: a software environment for integrated models of biomolecular interaction networks. Genome Res 2003; 13: 2498-2504.
[24] Chin CH, Chen SH, Wu HH, Ho CW, Ko MT and Lin CY. cytoHubba: identifying hub objects and sub-networks from complex interactome. BMC Syst Biol 2014; 8 Suppl 4: S11.
[25] Bader GD and Hogue CW. An automated method for finding molecular complexes in large protein interaction networks. BMC Bioinformatics 2003; 4: 2.
[26] Liang XZ, Luo D, Chen YR, Li JC, Yan BZ, Guo YB, Wen MT, Xu B and Li G. Identification of potential autophagy-related genes in steroid-induced osteonecrosis of the femoral head via bioinformatics analysis and experimental verification. J Orthop Surg Res 2022; 17: 86.
[27] Liu Y, Jia Y, Cao Y, Zhao Y, Du J, An F, Qi Y, Feng X, Jin T, Shi J and Wang J. MMP9 polymorphism is associated with susceptibility to non-traumatic osteonecrosis of femoral head in a Chinese Han population. Oncotarget 2017; 8: 82835-82841.
[28] Li T, Zhang Y, Wang R, Xue Z, Li S, Cao Y, Liu D, Niu Y, Mao X, Wang X, Li W, Guo Q, Guo M, Lin N and Chen W. Discovery and validation an eight-biomarker serum gene signature for the diagnosis of steroid-induced osteonecrosis of the femoral head. Bone 2019; 122: 199-208.
[29] Di Ceglie I, Ascone G, Cremers NAJ, Sloetjes AW, Walgreen B, Vogl T, Roth J, Verbeek JS, van de Loo FAJ, Koenders MI, van der Kraan PM, Blom AB, van den Bosch MHJ and van Lent PLEM. Fcγ receptor-mediated influx of S100A8/A9-producing neutrophils as inducer of bone erosion during antigen-induced arthritis. Arthritis Res Ther 2018; 20: 80.
[30] Wan C, Gilbert SR, Wang Y, Cao X, Shen X, Ramaswamy G, Jacobsen KA, Alaql ZS, Eberhardt AW, Gerstenfeld LC, Einhorn TA, Deng L and Clemens TL. Activation of the hypoxia-inducible factor-1alpha pathway accelerates bone regeneration. Proc Natl Acad Sci U S A 2008; 105: 686-691.
[31] Wang X, Dong C, Sun L, Zhu L, Sun C, Ma R, Ning K, Lu B, Zhang J and Xu J. Quantitative proteomic analysis of age-related subventricular zone proteins associated with neurodegenerative disease. Sci Rep 2016; 6: 37443.
[32] Watanabe M, Toyomura T, Wake H, Nishinaka T, Hatipoglu OF, Takahashi H, Nishibori M and Mori S. Identification of ribosomal protein L9 as a novel regulator of proinflammatory damage-associated molecular pattern molecules. Mol Biol Rep 2022; 49: 2831-2838.

A

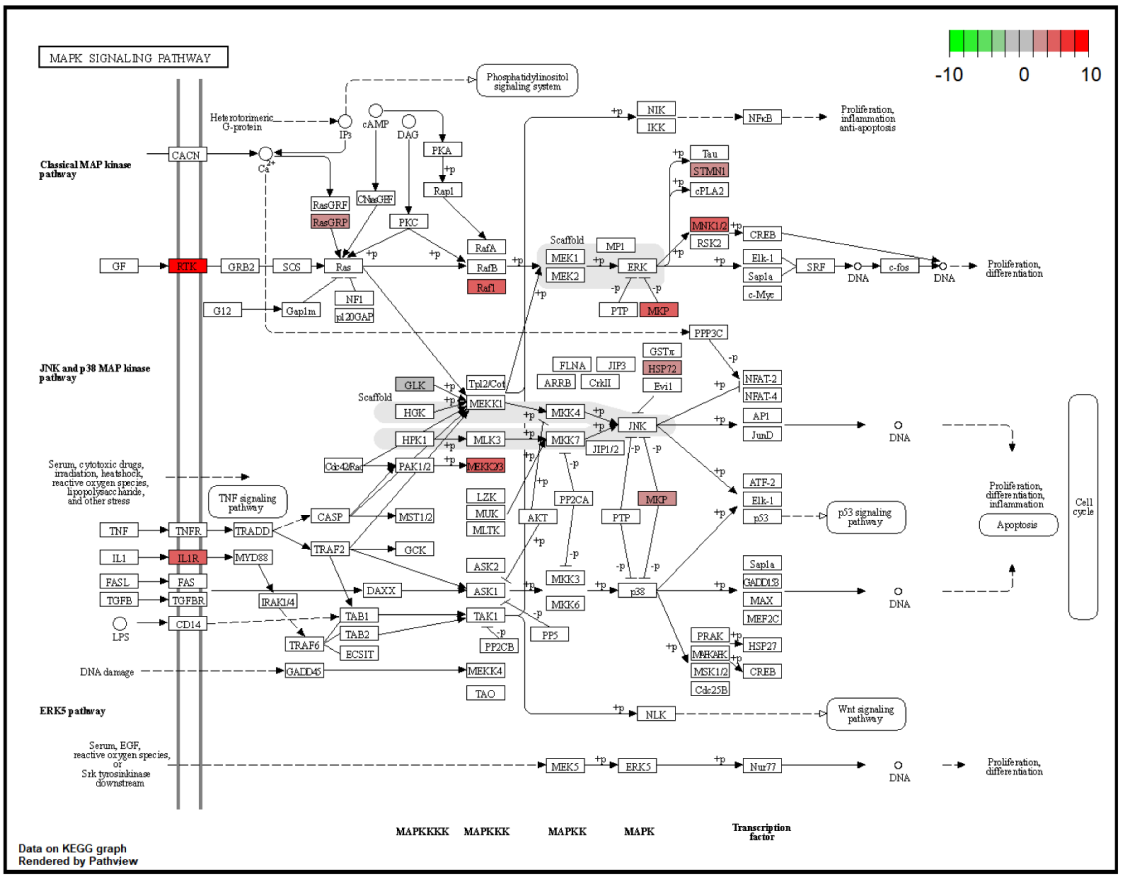
MAPK SIGNALING PATHWAY
-10
0
10
Classical MAP kinase pathway
JNK and p38 MAP kinase pathway
ERK5 pathway
MAPKKKK
MAPKKK
MAPKK
MAPK
Transcription factor
Data on KEGG graph
Rendered by Pathview

B

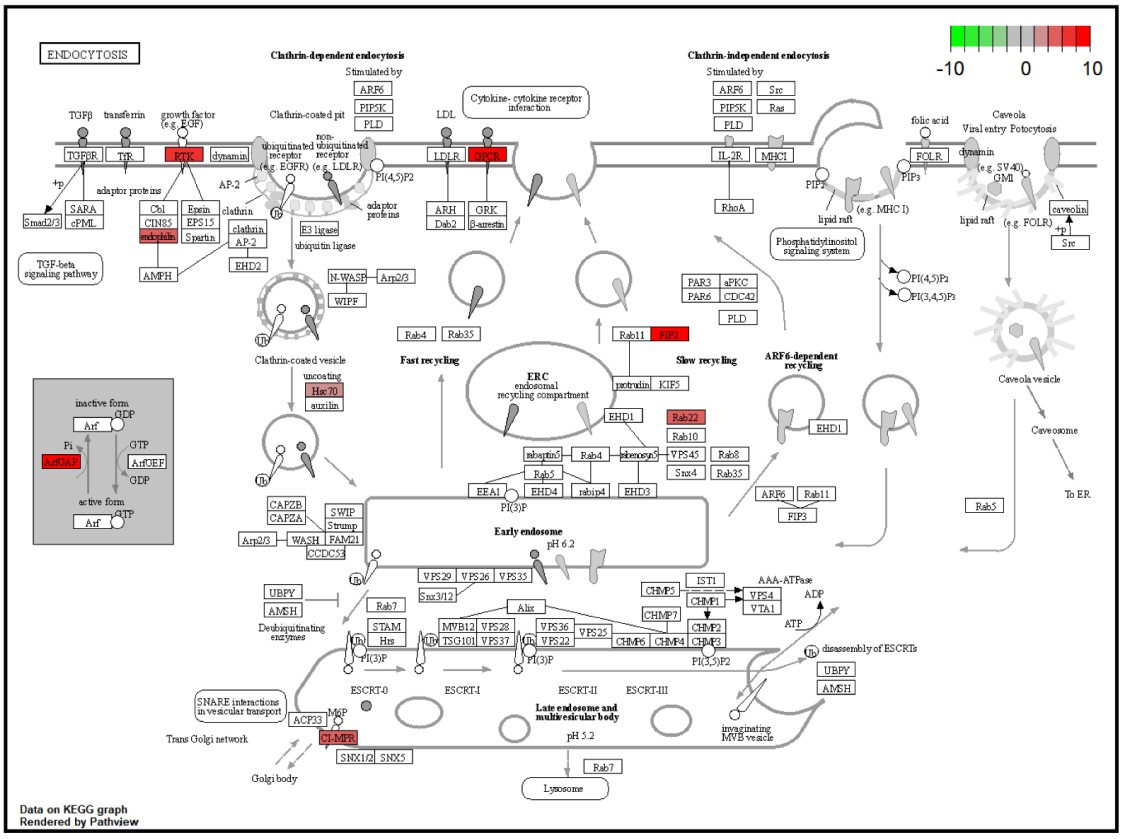
ENDOCYTOSIS
-10
0
10
Clathrin-dependent endocytosis
Clathrin-independent endocytosis
Caveola Viral entry Potocytosis
Fast recycling
Slow recycling
ARF6-dependent recycling
ERC
Early endosome
Late endosome and multivesicular body
ESCRT-0
ESCRT-I
ESCRT-II
ESCRT-III
Data on KEGG graph
Rendered by Pathview

Figure S1. Pathway diagram. A. MAPK Signaling pathway. B. Endocytosis pathway. Colors indicate differential expression; red denotes genes that are up-regulated, whereas green denotes genes that are down-regulated.

A

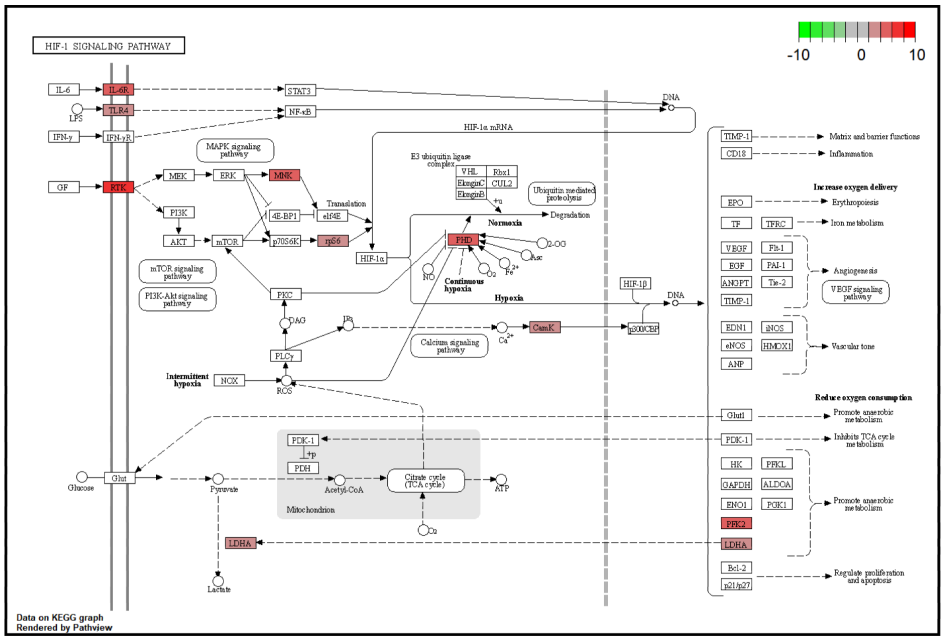

B

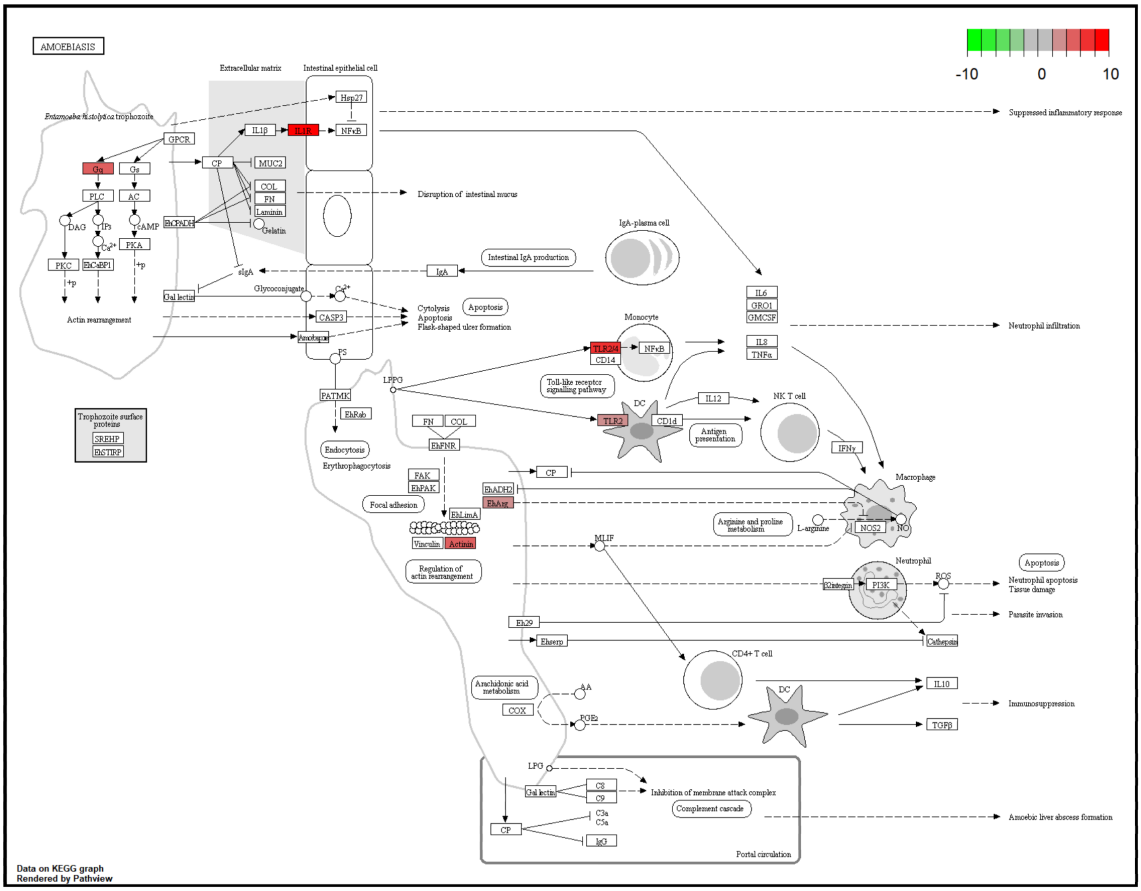

Figure S2. Pathway diagram. A. HIF-1 signaling pathway. B. Amoebiasis pathway. Colors indicate differential expression; red denotes genes that are up-regulated, whereas green denotes genes that are down-regulated.

A

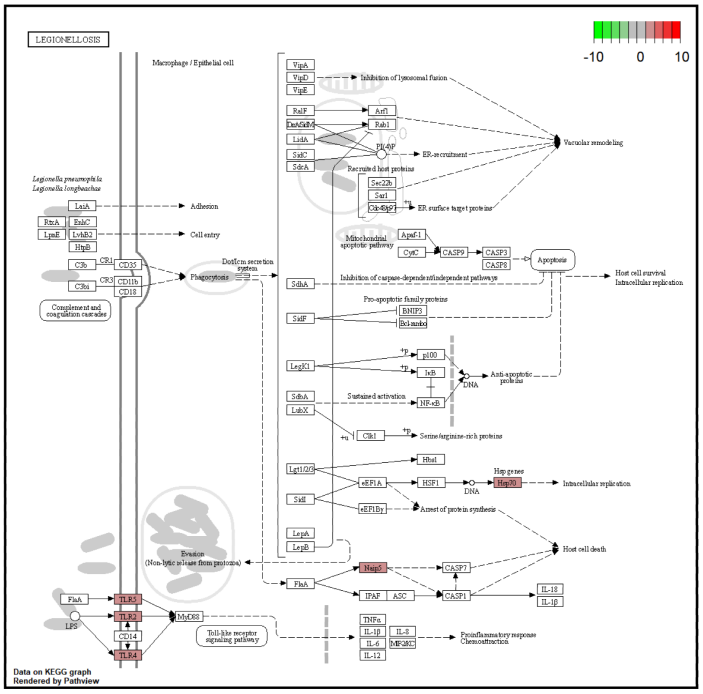

B

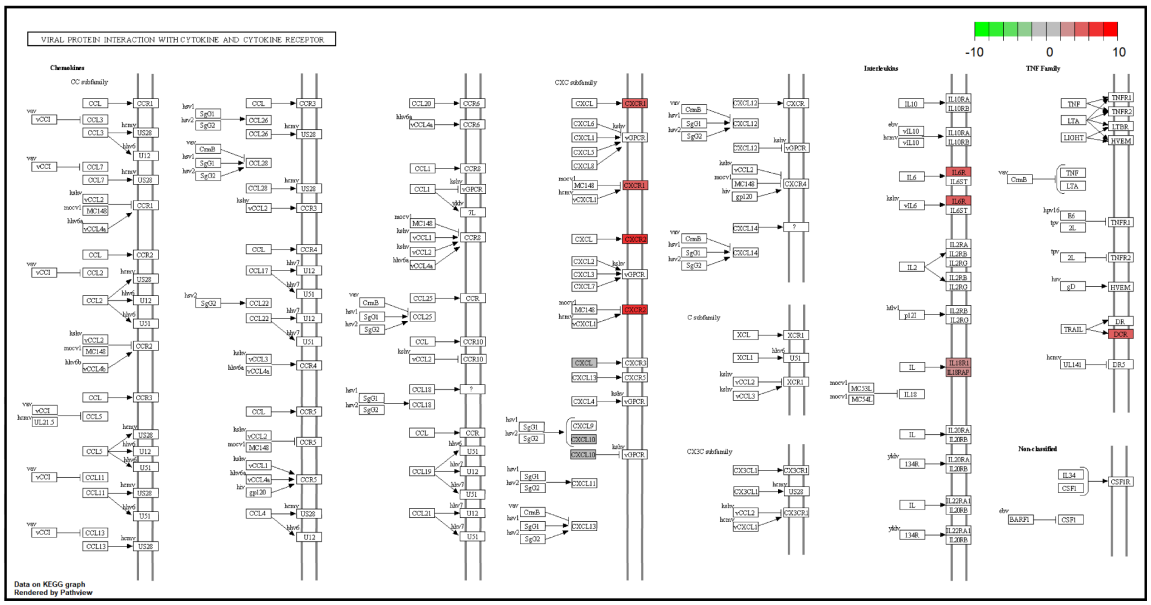

Figure S3. Pathway diagram. A. Legionellosis pathway. B. Viral protein interaction with cytokine and cytokine receptor. Colors indicate differential expression; red denotes genes that are up-regulated, whereas green denotes genes that are down-regulated.